

DRAFT VERSION JUNE 12, 2025
 Typeset using **L^AT_EX modern** style in AASTeX63

Thirty-Three New Stellar Angular Diameters from the NPOI, and Nearly 180 NPOI Diameters as an Ensemble

ELLYN K. BAINES,¹ JAMES H. CLARK III,¹ HENRIQUE R. SCHMITT,¹
 JORDAN M. STONE,¹ AND KASPAR VON BRAUN²

¹*Naval Research Laboratory, Remote Sensing Division, 4555 Overlook Ave SW, Washington, DC 20375, USA*

²*Lowell Observatory, 1400 W. Mars Hill Rd, Flagstaff, AZ 86001, USA*

ABSTRACT

We present new angular diameter measurements for 33 stars from the Navy Precision Optical Interferometer, reaching uncertainties on the limb-darkened diameter of 2% or less for 21 targets. We also determined the physical radius, bolometric flux, luminosity, and effective temperature for each star. Our sample is a mix of giant, subgiant, and dwarf stars, and span spectral classes from mid-A to mid-K. We combined these 33 stars with samples from previous publications to analyze how the NPOI diameters compare to those obtained using other means, namely ($V - K$) color, the *JMMC Stellar Diameters Catalog*, and *Gaia* predictions.

Keywords: stars: fundamental parameters, techniques: high angular resolution, techniques: interferometric

1. INTRODUCTION

In one sense, the story of astronomy can be told as the quest for better resolution: in its simplest form, the larger the telescope, the more detail you can see on a celestial object. At a certain point, extremely large telescope mirrors become incredibly complicated and prohibitively expensive to build, so we use telescope arrays to provide the ever-increasing resolution required. Optical and infrared interferometry has been used for some exciting explorations, including an expanding fireball from a nova explosion (Schaefer et al. 2014), observations of the dust sublimation region of a bright AGN Kishimoto et al. (2022), determining the size and thermal properties of an asteroid (Matter et al. 2013), supporting theoretical descriptions of a Mira variable star’s atmosphere (Wittkowski et al. 2016), and so on. Since its inception, optical and infrared interferometry has been used to measure stellar angular diameters (Michelson & Pease 1921; Wittkowski et al. 2001; van Belle et al. 2009;

(Boyajian et al. 2012a; Kervella et al. 2017, and many more), though these measurements are more generally the exception rather than the rule.

Stellar diameters have historically been determined using indirect methods, with photometry and spectroscopy being the most common. However, both of these techniques rely upon models of stellar interiors and atmospheres that cannot fully describe the complexity of the stars themselves. To make the models feasible, a number of simplifications and/or assumptions are required that we hope are mostly right, but some evidence shows they are not always accurate (e.g., Boyajian et al. 2012a, showed that models overestimate cooler stellar temperatures by $\sim 3\%$ and underestimate radii by $\sim 5\%$ for small stars. This paper also includes a discussion about the discrepancy between model predictions and direct measurements). Interferometric measurements are key to testing stellar models and acting as benchmarks (e.g., Perraut et al. 2020; Karovicova et al. 2020), which is particularly important in high signal-to-noise stellar spectroscopic studies and the *Gaia* survey. A collection of reliably calibrated stellar radii and effective temperatures based on accurate diameters is vital for their use in determining evolutionary state, understanding any planets orbiting the star, and calibrating empirical relationships such as the photometric color-temperature scale (Rains et al. 2020).

The angular diameter measurements presented here are a continuation of the survey project in Baines et al. (2018) and Baines et al. (2021), where we presented the angular diameters and other fundamental stellar properties for a total of 131 stars. This paper is organized as follows: Section 2 discusses the Navy Precision Optical Interferometer and the data reduction process; Section 3 describes interferometric visibility and calibration, Section 4 details how we determined various stellar parameters, including the radius, bolometric flux, extinction; luminosity, and effective temperature for each target; Section 5 provides notes on individual stars, when required; Section 6 considers NPOI angular diameters as an ensemble; and Section 7 is the conclusion.

2. INTERFEROMETRY WITH THE NPOI

As mentioned previously, one of the advantages that interferometry brings is its outstanding resolution, which can be an order of magnitude better than the largest telescopes equipped with adaptive optics (Rains et al. 2020). The Navy Precision Optical Interferometer (NPOI) is located on Anderson Mesa near Flagstaff, AZ (Armstrong et al. 1998; Hummel et al. 2003; Benson et al. 2003). It consists of three main arms, designated north, east, and west, and incorporates two sub-arrays: the four fixed astrometric stations concentrated near the center of the array (AC, AE, AW, and AN, which stand for astrometric center, east, west, and north, respectively), and the imaging stations. The latter are labeled according to which arm they are on and their relative distance from the array center. For example, E1 is the station nearest the center on the east arm, while E10 is the station farthest away. We can combine light from the astrometric and imaging stations at will, and “baseline” refers

to the distance between the two imaging elements. In this paper, we used 21 unique baselines, and Table 1 lists the baselines used and their average length. The minimum length of baseline used here was just under 9 m, while the longest was just over 79 m.

For the earliest data from 1996 to 2001, we used the original version of the “Classic” beam combiner that recorded data on one baseline per spectrograph, of which there were three, and the light was dispersed into 32 spectral channels spanning 450 to 950 nm. The data reduction for these early years follows procedures described in Hummel et al. (1998). For data from 2002 on, we used the updated “Classic” beam combiner that records data over 16 spectral channels across 550 to 850 nm (Hummel et al. 2003; Hutter et al. 2016). Every observation produced a pair of scans: a 30-second coherent (on the fringe) scan where the fringe contrast was measured every 2 ms, and an incoherent (off the fringe) scan that was used to estimate the additive bias affecting fringe measurements.

The NPOI’s data reduction package *OYSTER* was developed by C. A. Hummel¹ and automatically edits data as described in Hummel et al. (2003). In addition to this process, we edited out individual data points and/or scans that showed large scatter, on the order of 5σ or higher. This was more common in shorter-wavelength channels where the channels are narrower, atmospheric effects are more pronounced, and the avalanche photodiode detectors have lower quantum efficiency. We removed the points because while the diameter was not affected, the error determined using these points was unfairly biased by the lower-quality shorter-wavelength channels.

We made two assumptions about the stars at the outset: they are effectively single, and they do not rotate rapidly and therefore do not have an asymmetrical profile. Some of the targets measured here may have stellar companions, but almost all are comfortably outside of the detection sensitivity of the NPOI: Hutter et al. (2016) showed that the NPOI can detect binaries with separations from 3 to 860 mas with magnitude differences (Δm) of 3.0 for most binary systems, and up to 3.5 when the component spectral types differ by less than two. There are a few exceptions to these assumptions, which are discussed in Section 5.

Our end goal is to obtain angular diameters on the order of 2% or less, which is considered the minimal standard of astrophysically useful measurements (Booth 1997). Our sample consists of 30 stars with previously unpublished data in the NPOI data archive, and 3 stars observed solely in 2021, which were chosen for their large angular sizes (≥ 4 mas) due to the short baselines available at the time. The dates of observations range from 1996 to 2021, and the entire data set totals more than 56,000 data points. The smallest number of measurements for a given star is 102, and the largest is 6,529. Table 2 includes each target’s identifiers, spectral type, parallax, and metallicity ([Fe/H]), and Table 3 is the observing log.

¹ www.eso.org/~chummel/oyster/oyster.html

3. VISIBILITY & CALIBRATORS

Interferometric diameter measurements use visibility squared (V^2). For a point source, V^2 is 1 and it is defined as completely unresolved, while a star is completely resolved when its V^2 reaches zero. Atmospheric turbulence and instrumental effects can reduce the signal strength, significantly affecting V^2 . In order to address this, we used calibrator stars that are small, i.e., significantly less than the resolution of the NPOI, so that V^2 would be at or close to 1 and is only weakly dependent on the star's angular diameter. This means we can calibrate the atmospheric and instrumental variations out of the science target measurements as we observe calibrators and science targets alternately. The observations taken during a given night were obtained using the same configuration, and the time between data collection was generally on the order of a few minutes to 10 minutes.

To estimate the calibrators' diameters, we created spectral energy distribution (SED) fits to published *UBVRIJHK* photometry. We used plane-parallel model atmospheres from [Castelli & Kurucz \(2003\)](#) based on effective temperature (T_{eff}), surface gravity ($\log g$), and $E(B - V)$. Stellar models were fit to observed photometry after converting the magnitudes to fluxes using [Colina et al. \(1996\)](#) for *UBVRI* and [Cohen et al. \(2003\)](#) for *JHK*. Table 4 lists the photometry, T_{eff} , $\log g$, and $E(B - V)$ used, and the resulting angular diameters.²

Once the visibilities are calibrated, we fit angular diameters to the data. For a uniformly-illuminated disk, $V^2 = [2J_1(x)/x]^2$, where J_1 is the Bessel function of the first order, $x = \pi B \theta_{\text{UD}} \lambda^{-1}$, B is the projected baseline toward the star's position, θ_{UD} is the apparent uniform disk angular diameter of the star, and λ is the effective wavelength of the observation ([Shao & Colavita 1992](#)). θ_{UD} results for our program stars are listed in Table 5. The data are freely available in OIFITS form ([Duvert et al. 2017](#)) upon request.

We did not stop with the uniform disk diameter, though. A more realistic model of a star's disk includes limb darkening. When a linear limb darkening coefficient μ_{λ} is used, then

$$V^2 = \left(\frac{1 - \mu_{\lambda}}{2} + \frac{\mu_{\lambda}}{3} \right)^{-1} \times \left[(1 - \mu_{\lambda}) \frac{J_1(x_{\text{LD}})}{x_{\text{LD}}} + \mu_{\lambda} \left(\frac{\pi}{2} \right)^{1/2} \frac{J_{3/2}(x_{\text{LD}})}{x_{\text{LD}}^{3/2}} \right]^2, \quad (1)$$

where $x_{\text{LD}} = \pi B \theta_{\text{LD}} \lambda^{-1}$ and θ_{LD} is the limb darkened diameter ([Hanbury Brown et al. 1974a](#)). We gathered published T_{eff} , $\log g$, and $[\text{Fe}/\text{H}]$ values, and assigned a micro-turbulent velocity of 2 km s^{-1} to select μ_{λ} from [Claret & Bloemen \(2011\)](#). We used the ATLAS stellar model³ in the *R*-band, the waveband most closely matched to the central wavelength of the NPOI's bandpass. We note that a more refined analysis

² This is a simple SED fit, unlike the more sophisticated one described in Section 4. It is an appropriate method for calibrators, given the insensitivity of the target's measured angular diameter with respect to the calibrator's diameter ([Baines et al. 2018](#)).

³ The other choice was the PHOENIX model. We chose ATLAS because a range of metallicities were available as opposed to PHOENIX, which only had solar metallicity as an option.

would include limb darkening's non-linear dependence on wavelength, but believe the treatment described here is fair. Limb darkening effects are related to the height of the second maximum of the visibility curve (Wittkowski et al. 2001) and we deal almost entirely with measurements before the first minimum in this paper.

We calculated angular diameter uncertainties using the modified bootstrap Monte Carlo method developed by Tycner et al. (2010) where a large number of synthetic datasets are created by selecting entire scans at random, as opposed to a single data point within that scan. The width represents the standard deviation of the Gaussian distribution of diameters fit to these data sets, and it becomes our measure of the uncertainty for the diameter (see Figure 1).

For each target's data set, Table 5 shows the T_{eff} , $\log g$, [Fe/H], and μ_{λ} used, the resulting θ_{LD} , the maximum spatial frequency (SF), the number of scans, and the number of data points in the angular diameter fit. Figure 2 shows the θ_{LD} fit for HD 3712/ α Cas as an example. The remaining plots are included in the supplementary material of the *Astronomical Journal*.

4. STELLAR RADIUS, LUMINOSITY, AND EFFECTIVE TEMPERATURE

When available, we converted parallax from *Gaia* DR3 (Gaia Collaboration 2022) into a distance and combined it with our measured diameters to calculate the physical radius R . Otherwise, parallaxes from the *Hipparcos Astrometric Catalog* (van Leeuwen 2007), Mamajek & Hillenbrand (2008), and *Gaia* DR2 (Gaia Collaboration et al. 2018) were used, which was the case for 10 stars (see Table 2).

In order to determine each star's luminosity (L) and T_{eff} , we created SED fits using photometric and spectrophotometric values published in the sources listed in Table 6. The assigned uncertainties for the 2MASS infrared measurements are as reported in Cutri et al. (2003), and an uncertainty of 0.05 mag was assigned to the optical measurements. We did not use the R - and I -band data from (Ducati 2002) because they were always significant outliers.

We fit stellar spectral templates, interpolating when necessary, to the photometry from the flux-calibrated stellar spectral atlas of Pickles (1998) using the χ^2 minimization technique (Press et al. 1992; Wall & Jenkins 2003). This produced the bolometric flux (F_{BOL}) and extinction (A_{V}) for each star with the wavelength-dependent reddening relations of Cardelli et al. (1989). Next, we combined our F_{BOL} values with the stars' distances (d) to estimate L using $L = 4\pi d^2 F_{\text{BOL}}$. We also combined the F_{BOL} with θ_{LD} to determine each star's T_{eff} using the equation from van Belle et al. (1999):

$$F_{\text{BOL}} = \frac{1}{4} \theta_{\text{LD}}^2 \sigma T_{\text{eff}}^4, \quad (2)$$

where σ is the Stefan-Boltzmann constant and θ_{LD} is in radians (von Braun et al. 2014). The resulting R , F_{BOL} , A_{V} , T_{eff} , and L are listed in Table 7.

Because T_{eff} is an input to select μ_λ , we performed an iterative process to arrive at the final θ_{LD} . Table 5 shows the results of this process, including the initial θ_{LD} and subsequent T_{eff} , the recalculated μ_λ , and the final θ_{LD} and T_{eff} . For six stars, μ_λ and θ_{LD} did not change, and all of the remaining targets converged after just two iterations. Overall, μ_λ did not change much, with an average of 0.01 and a maximum of 0.06. The θ_{LD} changed by an average of 0.4% (0.012 mas) and a maximum of 2.3% (0.055 mas). Similarly, T_{eff} changed an average of 9 K, and at most 46 K.

Eight stars in this sample have never been measured before using interferometry (see Table 8), and Figure 3 compares our measurements with those that came before using a variety of instruments: the Two-Telescope Stellar Interferometer at CERGA, the Mark III, the NPOI, the Center for High Angular Resolution Astronomy (CHARA) Array, the Infrared Optical Telescope Array, the Stellar Intensity Interferometer at Narrabri, the Palomar Testbed Interferometer, and the Very Large Telescope Interferometer. There is generally good agreement across instruments and the wavebands they use.

5. NOTES ON INDIVIDUAL STARS

Some targets of interest include the following:

- *HD 62044/σ Gem*: This is a highly active single-lined spectroscopic RS CVn binary (Cao et al. 2022) with imaged star spots (Roettenbacher et al. 2017). The companion was resolved by Roettenbacher et al. (2015) but the magnitude difference between the components is too large to be detected by the NPOI at $Δm = 6.72$ (Mason et al. 2001). Roettenbacher et al. (2017) created temperature maps showing large star spots, though with much more tightly constrained interferometric measurements than we present here.
- *HD 102647/β Leo*: This young star is a favored target for exoplanet formation and evolution, considering it is one of the few known stars with hot, warm, and cold dust components with temperatures of $~1600$ K, 600 K, and 120 K, respectively (Chen et al. 2020). Defrère et al. (2021) studied β Leo with the Large Binocular Telescope Interferometer as part of the exozodical dust survey HOSTS. They discovered a dust level some 50 times greater than the one in our solar system’s zodiacal cloud, and concluded that any planet at about 5-50 AU must be less than a few Jupiter masses. They used the surface brightness relationships of Chelli et al. (2016) to determine a θ_{LD} of 1.43 ± 0.02 mas, versus our measurement of 1.479 ± 0.013 mas.

In addition to the dust components, β Leo is a δ Scuti variable and it shows pulsations, though of an unspecified type (Liakos & Niarchos 2017). It is also a multiple-star system, characterized by Rodriguez et al. (2015) as having an A-Ba pair with a separation of $1.91''$ and $Δm = 3.9$, and a Ba-Bb pair separated by $0.51''$ and $Δm = 0.129$. Between the magnitude difference of the A-B pair

and the fact that [van Belle & von Braun \(2009\)](#) considered the star a reliable star against which to compare exoplanet hosts, we treat our diameter as a single-star measurement.

- *HD 112185/ε UMa:* [Ludendorff \(1913\)](#) identified ϵ UMa as a spectroscopic binary over a hundred years ago, and [Roberts \(2011\)](#) identified a possible companion with a separation of $0.11''$ and $\Delta m = 2.31 \pm 0.03$ in the I -band. We did not see any evidence of a binary companion in our data, but plan on observing the star in the future in the hope of detecting (or not) the companion. Given that this star is bright at $V=1.77$, we would expect to see a companion with that separation easily.
- *HD 119228/83 UMa:* A suspected non-single and problem *Hipparcos* binary ([Mason et al. 1999](#)), [Horch et al. \(2017\)](#) observed 83 UMa with Differential Speckle Survey Instrument on the WIYN telescope, and did not detect any companions. They derived a detection limit as a function of separation and found that the Δm at both $0.2''$ and $1.0''$ ($\Delta m = 4.36$ and 7.55 , respectively, at 692 nm, and 3.92 and 7.30, respectively, at 880 nm) would be well beyond the detection limit of the NPOI.
- *HD 124850/ι Vir:* [Raghavan et al. \(2010\)](#) synthesized previous information on the question of whether ι Vir is single or binary, and concluded “single, candidate binary” and retained it as an object for future exploration. [Raghavan et al. \(2012\)](#) later used the CHARA Array to look for previously unknown companions to nearby solar-type stars to help fill the gap between spectroscopic and visual techniques. They explored the 8-80 mas range in a search for separated fringe packets, and did not find any indication of a companion for ι Vir. They again labeled it as maybe having a companion with a 55 year orbit, and we treat the star as single here.
- *HD 173764/β Sct:* The always informative and often entertaining [Griffin \(2008\)](#) analyzed β Sct’s binary nature and determined an orbit of $P = 833.26 \pm 0.07$ d. He discussed the confusion arising due to the secondary’s nature, considering it is bright in ultraviolet but its contribution to the total luminosity is very small in optical wavelengths, on the order of $\Delta m = 4\text{-}5$ in the V -band. [Hutter et al. \(2016\)](#) used the NPOI to detect the secondary component for the first time at precisely measured separations and position angles. The Δm of $3.6_{-0.1}^{+0.2}$ at 700 nm is on the very edge of what the NPOI can detect.
- *HD 183912/β Cyg A:* Part of the beautiful and increasingly complicated Albireo star system ([Mason et al. 2001](#), see especially the rich collection of stars in the Washington Double Star Catalog), Albireo was measured by [Mozurkewich et al. \(2003\)](#) as a single star with $\theta_{LD} = 4.834 \pm 0.048$ mas. More recently, [Drimmel et al. \(2021\)](#) used spectroscopy to determine the all three stars in

the system (Aa, Ac, and B) are likely coeval and in a hierarchical triple system with an orbital period of $121.65^{+3.34}_{-2.90}$ years. They speculated that Alberio is not done with its surprises yet in the form of an undetected fourth companion. [Jack et al. \(2022\)](#) found evidence of that star, Ad, with a period of ~ 371 d and a mass of $0.085 M_{\odot}$. We did not yet search for a binary signal in the NPOI data and present the diameter as if for a single star.

- *HD 198149/η Cep:* [Hutter et al. \(2016\)](#) obtained some tantalizing but borderline indications of binarity for this target. Of the three nights they used in their analysis, the binary model fit best for one night, marginally better for the second, and the third was better fit with a single-star model. We treat the star as single here, with our older (1997) data, and look forward to future observations and a better determination of the single or binary state of the target.
- *HD 203280/α Cep/Alderamin:* [van Belle et al. \(2006\)](#) used the CHARA Array to characterize Alderamin as a rapid rotator with a measurable oblateness between the polar angular diameter of 1.355 ± 0.009 mas and the equatorial diameter of 1.625 ± 0.050 mas. This produced a rotational velocity of 283 ± 10 km s⁻¹, which is 83% of the breakup velocity. Also of note are the images and gravity darkening models of Alderamin made by [Zhao et al. \(2009\)](#) also made using the CHARA Array, which showed the star has two hotter, bright polar areas and a cooler, darker equator. Both sets of CHARA measurements had the advantage of better coverage around the limb of the star, more than the NPOI measurements presented here, which do not have the coverage required to detect asymmetries for this target. Our θ_{LD} of 1.674 ± 0.008 mas most likely corresponds more closely to the equatorial diameter measurement, by chance.
- *HD 221115/70 Peg:* [Griffin \(2009\)](#) provides the orbit for this spectroscopic binary, and notes the spectral types as G8 III for the primary and as late as M2 V for the secondary. This is beyond the sensitivity of the NPOI to detect, so we present the angular diameter as a single star.
- *HD 222107/λ And:* A chromospherically active giant RS CVn star, ([Parks et al. 2021](#)) imaged cool starspots using CHARA Array data from 2010 and 2011. [Martinez et al. \(2021\)](#) used the same data to reconstruct temperature maps. Both teams also measured the angular diameter of the primary star, effectively single at the detection limits of interferometry, of 2.759 ± 0.050 mas and 2.742 ± 0.010 mas, respectively. These agree well with our measurement of 2.769 ± 0.012 mas, though the data we used from 1997 only used three telescopes (instead of the six in the CHARA studies), so we lack the coverage to produce surface maps.
- *HD 224014/ρ Cas:* This star is one of the Big Three yellow hypergiants, with the other two being HR 8752/V509 Cas and HR 5171A/V766 Cen

(van Genderen et al. 2019, and references therein). These stars are characterized by being almost entirely convective with very extended atmospheres, having surface gravities near zero, and showing high mass-loss rates. They exhibit pulsations on quasi-periods of a few hundred days, with a pattern that shows a “coherent sequence of pulsations, but that each pulsation is unique.” Because of this, an SED fit would need to be better tailored to an ever-changing target, and general photometry from the literature is too smeared out to be precise. We include the angular diameter and radius in Tables 5 and 7, but do not continue with the T_{eff} calculation. We also note that the phase may affect our diameter measurement, if the pulsation amplitude is significantly larger than the random error.

We used the parallax from the earlier *Gaia* release (0.947 ± 0.202 mas, Gaia Collaboration et al. 2018) because using the more recent value from Gaia Collaboration (2022) of -0.057 ± 0.0945 mas produced a radius of over $4,500 R_{\odot}$, and we do not claim that as real.

6. PAST AND PRESENT NPOI DIAMETERS

When we combine these stars with NPOI angular diameters from previous samples from Baines et al. (2014), Baines et al. (2018), Baines et al. (2021), and Baines et al. (2023), we end up with 178 stars (see Table 9). Figure 4 shows a color-magnitude diagram for the current and previous NPOI diameters along with targets within the NPOI observing range (declination ≥ -10 deg and $V \leq 6.0$) from the *JMMC Stellar Diameters Catalog* (Bourg  s et al. 2014). With a collection on this scale, we can investigate some relationships in a more quantitative sense.

We began with the equations from Mozurkewich et al. (2003) linking colors to surface brightness (S_V):

$$S_V = m_V + 5 \log(\theta_{\text{LD}}), \quad (3)$$

where m_V is the apparent visual magnitude, and

$$S_V = 2.658 + 1.385(V - K) - 0.021(V - K)^2. \quad (4)$$

We dereddened the V magnitudes from Mermilliod (1991) using A_V listed in Table 9 and used Equations 3 and 4 to estimate θ_{LD} from $(V - K)$ with K magnitudes from Cutri et al. (2003) except for the stars HD189319/   Sge and HD 192909/32 Cyg, which did not have 2MASS measurements. For these, we used K magnitudes from Richichi & Percheron (2005) and assigned an error of 0.01 mag because none was specified. Table 9 includes the resulting diameters, and Figure 5 shows the

result of the fit. There is excellent agreement within about 1%, with a linear fit of $f(x) = 1.001x + 0.068$.⁴

We went through the same procedure with the angular diameter-color relations in Adams et al. (2018), who used a sample of dwarfs/subgiants and a sample of giant stars to fit empirical relations of angular diameters to various colors, including $(V - I_C)$, $(V - H)$, $(V - K)$, $(I_C - H)$, and $(I_C - K)$. Because the relations are limited to the color ranges for which they had data, we did not use all of our 178 stars: 54 of our stars were out of range while 124 were within the limits. We used the coefficients appropriate for the luminosity class of each star, and obtained a fit of $f(x) = 1.039x - 0.014$ (see Figure 6). Adams et al. provided a range of predicted fractional uncertainty, which we averaged and applied to the diameters: 3.6% for giant stars, and 3.0% for dwarf and subgiant stars.

We also compared angular diameters from the *JMMC Stellar Diameters Catalogue* (Bourg  s et al. 2014), and estimates from the *Gaia* catalog (Cruzal  bes et al. 2013, derived from radii and distances from *Gaia* Collaboration et al. 2018). Figure 7 shows this in graphical form, with the *JMMC* diameters compared in the top panel and the *Gaia* diameters in the bottom panel. The *JMMC* diameters show a reasonable fit overall, with a linear fit of $f(x) = 0.969x + 0.088$, while the *Gaia* comparison shows more scatter. The fit is good with a larger y-intercept at $f(x) = 0.996x + 0.246$, so the information could be useful for ensembles of stars, but not for an individual comparison. Cruzal  bes et al. note this issue as well, explaining that the diameters were determined using only three broad-band photometric measurements, which show strong degeneracies between T_{eff} and extinction/reddening meaning “strong assumptions” are required.

7. CONCLUSION

We measured angular diameters for 33 stars from 0.715 mas to 10.144 mas. The former has an uncertainty of ± 0.205 mas (29%), while the latter has an uncertainty of ± 0.020 mas (0.2%). Of the 33 stars presented here, all but six targets have diameter uncertainties of $\leq 5\%$, and all but 12 stars have uncertainties of $\leq 2\%$. We present six stars close to 1.0 mas or smaller, which is under the formal resolution limit of the NPOI. It is therefore not surprising that those uncertainties are amongst the highest.

We also combined diameters from four other NPOI papers containing angular diameters to assess the collection as a whole, and compared our diameters to those obtained using other methods.

ACKNOWLEDGMENTS

⁴ The star HD 42995/ η Gem was removed for the fit because the $(V-K)$ diameter produced 14.07 ± 1.02 mas while the NPOI measurement is 12.112 ± 0.024 mas. When this star was included, the linear fit was $f(x) = 0.978x + 0.135$. The uncertainties in the slope and intercept are $f(x) = 0.978 \pm 0.012 + 0.136 \pm 0.052$ with HD 42995, and $f(x) = 1.006 \pm 0.012 + 0.069 \pm 0.050$ without it.

The Navy Precision Optical Interferometer is a joint project of the Naval Research Laboratory and the U.S. Naval Observatory, and is funded by the Office of Naval Research and the Oceanographer of the Navy. This research has made use of the SIMBAD database and Vizier catalogue access tool, operated at CDS, Strasbourg, France. This publication made use of data products from the Two Micron All Sky Survey, which is a joint project of the University of Massachusetts and the Infrared Processing and Analysis Center/California Institute of Technology, funded by the National Aeronautics and Space Administration and the National Science Foundation. This research has made use of the Jean-Marie Mariotti Center JSDC catalogue, available at http://www.jmmc.fr/catalogue_jsdc.htm.

REFERENCES

- Adams, A. D., Boyajian, T. S., & von Braun, K. 2018, MNRAS, 473, 3608.
doi:10.1093/mnras/stx2367
- Akeson, R. L., Ciardi, D. R., Millan-Gabet, R., et al. 2009, ApJ, 691, 1896.
doi:10.1088/0004-637X/691/2/1896
- Alekseeva, G. A., Arkharov, A. A., Galkin, V. D., et al. 1997, VizieR Online Data Catalog, III/201
- Alexander, J. B., Jones, D. H. P., & Sinclair, J. E. 1983, RGOB, 191, 1A
- Allende Prieto, C., & Lambert, D. L. 1999, A&A, 352, 555.
doi:10.48550/arXiv.astro-ph/9911002
- Alonso, A., Arribas, S., & Martinez-Roger, C. 1996, A&AS, 117, 227
- Anderson, E. & Francis, C. 2012, Astronomy Letters, 38, 331.
doi:10.1134/S1063773712050015
- Armstrong, J. T., Mozurkewich, D., Rickard, L. J., et al. 1998, ApJ, 496, 550. doi:10.1086/305365
- Baines, E. K., Armstrong, J. T., Clark, J. H., et al. 2021, AJ, 162, 198.
doi:10.3847/1538-3881/ac2431
- Baines, E. K., Armstrong, J. T., Schmitt, H. R., et al. 2014, ApJ, 781, 90.
doi:10.1088/0004-637X/781/2/90
- Baines, E. K., Armstrong, J. T., Schmitt, H. R., et al. 2018, AJ, 155, 30.
doi:10.3847/1538-3881/aa9d8b
- Baines, E. K., Blomquist, S., Clark, J. H., et al. 2023, AJ, 165, 41.
doi:10.3847/1538-3881/aca277
- Benson, J. A., Hummel, C. A., & Mozurkewich, D. 2003, Proc. SPIE, 4838, 358. doi:10.1117/12.459322
- Bonneau, D., Koechlin, L., Oneto, J. L., et al. 1981, A&A, 103, 28
- Booth, A. J. 1997, IAU Symposium, 189, 147
- Bourg  s, L., Lafrasse, S., Mella, G., et al. 2014, Astronomical Data Analysis Software and Systems XXIII, 485, 223
- Boyajian, T. S., McAlister, H. A., van Belle, G., et al. 2012b, ApJ, 746, 101.
doi:10.1088/0004-637X/746/1/101
- Boyajian, T. S., von Braun, K., van Belle, G., et al. 2012a, ApJ, 757, 112.
doi:10.1088/0004-637X/757/2/112
- Burnashev, B. I. 1985, Bulletin Crimean Astrophysical Observatory, 66, 152
- Cao, D., Gu, S., Grundahl, F., et al. 2022, MNRAS, 514, 4190.
doi:10.1093/mnras/stac1576
- Cardelli, J. A., Clayton, G. C., & Mathis, J. S. 1989, ApJ, 345, 245
- Castelli, F. & Kurucz, R. L. 2003, Modelling of Stellar Atmospheres, 210, A20.
doi:10.48550/arXiv.astro-ph/0405087
- Chelli, A., Duvert, G., Bourg  s, L., et al. 2016, A&A, 589, A112.
doi:10.1051/0004-6361/201527484

- Chen, X., Ge, Z., Chen, Y., et al. 2020, *ApJ*, 889, 157.
doi:10.3847/1538-4357/ab66c7
- Claret, A., & Bloemen, S. 2011, *A&A*, 529, A75.
doi:10.1051/0004-6361/201116451
- Clem, J. L., VandenBerg, D. A., Grundahl, F., et al. 2004, *AJ*, 127, 1227. doi:10.1086/381295
- Cohen, M., Wheaton, W. A., & Megeath, S. T. 2003, *AJ*, 126, 1090.
doi:10.1086/376474
- Colina, L., Bohlin, R. C., & Castelli, F. 1996, *AJ*, 112, 307. doi:10.1086/118016
- Cruzalèbes, P., Jorissen, A., Rabbia, Y., et al. 2013, *MNRAS*, 434, 437.
doi:10.1093/mnras/stt1037
- Cruzalèbes, P., Petrov, R. G., Robbe-Dubois, S., et al. 2019, *MNRAS*, 490, 3158. doi:10.1093/mnras/stz2803
- Cutri, R. M., Skrutskie, M. F., van Dyk, S., et al. 2003, *VizieR Online Data Catalog*, II/246
- Defrère, D., Hinz, P. M., Kennedy, G. M., et al. 2021, *AJ*, 161, 186.
doi:10.3847/1538-3881/abe3ff
- Di Folco, E., Thévenin, F., Kervella, P., et al. 2004, *A&A*, 426, 601.
doi:10.1051/0004-6361:20047189
- Drimmel, R., Sozzetti, A., Schröder, K.-P., et al. 2021, *MNRAS*, 502, 328.
doi:10.1093/mnras/staa4038
- Ducati, J. R. 2002, *VizieR Online Data Catalog*, II/237
- Duvert, G., Young, J., & Hummel, C. A. 2017, *A&A*, 597, A8.
doi:10.1051/0004-6361/201526405
- Dyck, H. M., Benson, J. A., van Belle, G. T., et al. 1996, *AJ*, 111, 1705.
doi:10.1086/117910
- Dyck, H. M., van Belle, G. T., & Thompson, R. R. 1998, *AJ*, 116, 981.
doi:10.1086/300453
- Famaey, B., Jorissen, A., Luri, X., et al. 2005, *A&A*, 430, 165.
doi:10.1051/0004-6361:20041272
- Faucherre, M., Bonneau, D., Koechlin, L., et al. 1983, *A&A*, 120, 263
- Friedemann, C. 1992, *Bulletin d'Information du Centre de Donnees Stellaires*, 40, 31
- Gaia Collaboration, Brown, A. G. A., Vallenari, A., et al. 2018, *A&A*, 616, A1. doi:10.1051/0004-6361/201833051
- Gaia Collaboration 2022, *VizieR Online Data Catalog*, I/355
- Gáspár, A., Rieke, G. H., & Ballering, N. 2016, *ApJ*, 826, 171.
doi:10.3847/0004-637X/826/2/171
- Gebran, M., Farah, W., Paletou, F., et al. 2016, *A&A*, 589, A83.
doi:10.1051/0004-6361/201528052
- Gezari, D. Y., Pitts, P. S., & Schmitz, M. 1999, *VizieR Online Data Catalog*, II/225
- Gezari, D. Y., Schmitz, M., Pitts, P. S., & Mead, J. M. 1993, *Catalog of Infrared Observations*, NASA Reference Publication 1294 (3rd ed.; Greenbelt, MD: NASA)
- Glushneva, I. N., Doroshenko, V. T., Fetisova, T. S., et al. 1998, *VizieR Online Data Catalog*, III/208
- Golay, M. 1972, *Vistas in Astronomy*, 14, 13. doi:10.1016/0083-6656(72)90023-2
- Gontcharov, G. A. & Mosenkov, A. V. 2018, *VizieR Online Data Catalog*, II/354
- Griffin, R. F. 2008, *The Observatory*, 128, 21
- Griffin, R. F. 2009, *The Observatory*, 129, 198
- Häggkvist, L. & Oja, T. 1970, *A&AS*, 1, 199
- Hanbury Brown, R., Davis, J., & Allen, L. R. 1974b, *MNRAS*, 167, 121.
doi:10.1093/mnras/167.1.121
- Hanbury Brown, R., Davis, J., Lake, R. J. W., & Thompson, R. J. 1974a, *MNRAS*, 167, 475.
doi:10.1093/mnras/167.3.475
- Helou, G. & Walker, D. W. 1988, *Infrared astronomical satellite (IRAS) catalogs and atlases. Volume 7*, 7, 1
- Høg, E., Fabricius, C., Makarov, V. V., et al. 2000, *A&A*, 355, L27

- Horch, E. P., Casetti-Dinescu, D. I., Camarata, M. A., et al. 2017, AJ, 153, 212. doi:10.3847/1538-3881/aa6749
- Huang, W., Gies, D. R., & McSwain, M. V. 2010, ApJ, 722, 605. doi:10.1088/0004-637X/722/1/605
- Hummel, C. A., Benson, J. A., Hutter, D. J., et al. 2003, AJ, 125, 2630. doi:10.1086/374572
- Hummel, C. A., Mozurkewich, D., Armstrong, J. T., et al. 1998, AJ, 116, 2536. doi:10.1086/300602
- Hunter, I., Smoker, J. V., Keenan, F. P., et al. 2006, MNRAS, 367, 1478. doi:10.1111/j.1365-2966.2006.10054.x
- Hutter, D. J., Zavala, R. T., Tycner, C., et al. 2016, ApJS, 227, 4. doi:10.3847/0067-0049/227/1/4
- Jack, D., Schröder, K.-P., Mittag, M., et al. 2022, A&A, 661, A49. doi:10.1051/0004-6361/202243255
- Jenkins, E. B. 2009, ApJ, 700, 1299. doi:10.1088/0004-637X/700/2/1299
- Johnson H.L. 1963, Tonantzintla Tacubaya 3, 305
- Johnson, H. L. & Mitchell, R. I. 1975, RMxAA, 1, 299
- Kakaras, G., Straizys, V., Sudzius, J., & Zdanavicius, K. 1968, Vilnius Astronomijos Observatorijos Biuletenis, 22, 3.
- Karovicova, I., White, T. R., Nordlander, T., et al. 2020, A&A, 640, A25. doi:10.1051/0004-6361/202037590
- Kervella, P., Bigot, L., Gallenne, A., & Thévenin, F. 2017, A&A, 597, A137
- Kharitonov, A. V., Tereshchenko, V. M., & Knyazeva, L. N. 1988, The spectrophotometric catalogue of stars. Book of reference. (The spectrophotometric catalogue of stars. Book of reference., by Kharitonov, A. V.; Tereshchenko, V. M.; Knyazeva, L. N.. Nauka, Alma-Ata (USSR), 1988, 478 p., ISBN 5-628-00165-1, Price 4 Rbl. 80 Kop.)
- Kishimoto, M., Anderson, M., ten Brummelaar, T., et al. 2022, ApJ, 940, 28. doi:10.3847/1538-4357/ac91c4
- Koleva, M. & Vazdekis, A. 2012, A&A, 538, A143. doi:10.1051/0004-6361/201118065
- Kornilov, V. G., Volkov, I. M., Zakharov, A. I., Kozyreva, L. N., Kornilova, L. N., & et al. 1991, Trudy Gosudarstvennogo Astronomicheskogo Instituta, 63, 4
- Le Borgne, J.-F., Bruzual, G., Pelló, R., et al. 2003, A&A, 402, 433. doi:10.1051/0004-6361:20030243
- Liakos, A. & Niarchos, P. 2017, MNRAS, 465, 1181. doi:10.1093/mnras/stw2756
- Ludendorff, H. 1913, Astronomische Nachrichten, 195, 369. doi:10.1002/asna.19131951902
- Mamajek, E. E. & Hillenbrand, L. A. 2008, ApJ, 687, 1264. doi:10.1086/591785
- Martinez, A. O., Baron, F. R., Monnier, J. D., et al. 2021, ApJ, 916, 60. doi:10.3847/1538-4357/ac06a5
- Mason, B. D., Martin, C., Hartkopf, W. I., et al. 1999, AJ, 117, 1890. doi:10.1086/300823
- Mason, B. D., Wycoff, G. L., Hartkopf, W. I., et al. 2001, AJ, 122, 3466. doi:10.1086/323920
- Matter, A., Delbo, M., Carry, B., et al. 2013, Icarus, 226, 419. doi:10.1016/j.icarus.2013.06.004
- McDonald, I., Zijlstra, A. A., & Watson, R. A. 2017, MNRAS, 471, 770. doi:10.1093/mnras/stx1433
- Mendoza, E. E. 1967, Boletin de los Observatorios Tonantzintla y Tacubaya, 4, 149
- Mermilliod, J.-C. 1987, A&AS, 71, 413
- Mermilliod, J.-C. 1991, *Catalogue of Homogeneous Means in the UBV System*, Institut d'Astronomie, Universite de Lausanne
- Mermilliod, J.-C. & Nitschelm, C. 1989, A&AS, 81, 401
- Michelson, A. A. & Pease, F. G. 1921, ApJ, 53, 249. doi:10.1086/142603
- Monet, D. G., Levine, S. E., Canzian, B., et al. 2003, AJ, 125, 984. doi:10.1086/345888
- Morel, M. & Magnenat, P. 1978, A&AS, 34, 477

- Mozurkewich, D., Armstrong, J. T., Hindsley, R. B., et al. 2003, AJ, 126, 2502. doi:10.1086/378596
- Mozurkewich, D., Johnston, K. J., Simon, R. S., et al. 1991, AJ, 101, 2207. doi:10.1086/115843
- Neckel, T., Klare, G., & Sarcander, M. 1980, Bulletin d'Information du Centre de Donnees Stellaires, 19, 61
- Nordgren, T. E., Germain, M. E., Benson, J. A., et al. 1999, AJ, 118, 3032. doi:10.1086/301114
- Nordgren, T. E., Sudol, J. J., & Mozurkewich, D. 2001, AJ, 122, 2707. doi:10.1086/323546
- Otte, B., & Dixon, W. V. D. 2006, ApJ, 647, 312. doi:10.1086/505414
- Parks, J. R., White, R. J., Baron, F., et al. 2021, ApJ, 913, 54. doi:10.3847/1538-4357/abb670
- Perraut, K., Cunha, M., Romanovskaya, A., et al. 2020, A&A, 642, A101. doi:10.1051/0004-6361/202038753
- Perrin, G., Coudé du Foresto, V., Ridgway, S. T., et al. 1998, A&A, 331, 619
- Pickles, A. J. 1998, PASP, 110, 863
- Press, W. H., Teukolsky, S. A., Vetterling, W. T., & Flannery, B. P. 1992, Numerical recipes in C. The art of scientific computing (Cambridge: University Press, c1992, 2nd ed.)
- Prugniel, P., Soubiran, C., Koleva, M., & Le Borgne, D. 2007, arXiv:astro-ph/0703658
- Raghavan, D., Farrington, C. D., ten Brummelaar, T. A., et al. 2012, ApJ, 745, 24. doi:10.1088/0004-637X/745/1/24
- Raghavan, D., McAlister, H. A., Henry, T. J., et al. 2010, ApJS, 190, 1. doi:10.1088/0067-0049/190/1/1
- Rains, A. D., Ireland, M. J., White, T. R., et al. 2020, MNRAS, 493, 2377. doi:10.1093/mnras/staa282
- Richichi, A. & Percheron, I. 2005, A&A, 434, 1201. doi:10.1051/0004-6361:20042257
- Richichi, A., Percheron, I., & Khristoforova, M. 2005, A&A, 431, 773. doi:10.1051/0004-6361:20042039
- Roberts, L. C. 2011, MNRAS, 413, 1200. doi:10.1111/j.1365-2966.2011.18205.x
- Robin, A. C., Luri, X., Reylé, C., et al. 2012, A&A, 543, A100. doi:10.1051/0004-6361/201118646
- Rodriguez, D. R., Duchêne, G., Tom, H., et al. 2015, MNRAS, 449, 3160. doi:10.1093/mnras/stv483
- Roettenbacher, R. M., Monnier, J. D., Henry, G. W., et al. 2015, ApJ, 807, 23. doi:10.1088/0004-637X/807/1/23
- Roettenbacher, R. M., Monnier, J. D., Korhonen, H., et al. 2017, ApJ, 849, 120. doi:10.3847/1538-4357/aa8ef7
- Salsi, A., Nardetto, N., Mourard, D., et al. 2020, A&A, 640, A2. doi:10.1051/0004-6361/202038012 969 x + 0.088
- Sánchez-Blázquez, P., Peletier, R. F., Jiménez-Vicente, J., et al. 2006, MNRAS, 371, 703. doi:10.1111/j.1365-2966.2006.10699.x
- Schaefer, G. H., Brummelaar, T. T., Gies, D. R., et al. 2014, Nature, 515, 234. doi:10.1038/nature13834
- Shao, M., & Colavita, M. M. 1992, ARA&A, 30, 457. doi:10.1146/annurev.aa.30.090192.002325
- Smith, B. J., Price, S. D., & Baker, R. I. 2004, ApJS, 154, 673. doi:10.1086/423248
- Soubiran, C., Le Campion, J.-F., Brouillet, N., & Chemin, L. 2016, A&A, 591, A118. doi:10.1051/0004-6361/201628497
- Straizys, V., Kazlauskas, A., Jodinskiene, E., et al. 1995, VizieR Online Data Catalog, II/157A
- Tycner, C., Hutter, D. J., & Zavala, R. T. 2010, Proc. SPIE, 7734, 103T. doi:10.1117/12.857345
- Valdes, F., Gupta, R., Rose, J. A., Singh, H. P., & Bell, D. J. 2004, ApJS, 152, 251. doi:10.1086/386343
- van Belle, G. T., Ciardi, D. R., ten Brummelaar, T., et al. 2006, ApJ, 637, 494. doi:10.1086/498334

- van Belle, G. T., Creech-Eakman, M. J., & Hart, A. 2009, MNRAS, 394, 1925.
doi:10.1111/j.1365-2966.2008.14146.x
- van Belle, G. T., Lane, B. F., Thompson, R. R., et al. 1999, AJ, 117, 521
- van Belle, G. T., van Belle, G., Creech-Eakman, M. J., et al. 2008, ApJS, 176, 276-292. doi:10.1086/526548
- van Belle, G. T. & von Braun, K. 2009, ApJ, 694, 1085.
doi:10.1088/0004-637X/694/2/1085
- van Genderen, A. M., Lobel, A., Nieuwenhuijzen, H., et al. 2019, A&A, 631, A48.
doi:10.1051/0004-6361/201834358
- van Leeuwen, F. 2007, A&A, 474, 653.
doi:10.1051/0004-6361:20078357
- von Braun, K., Boyajian, T. S., van Belle, G. T., et al. 2014, MNRAS, 438, 2413.
doi:10.1093/mnras/stt2360
- Wall, J. V., & Jenkins, C. R. 2003, Practical Statistics for Astronomers, Cambridge Observing Handbooks for Research Astronomers, vol. 3. (Cambridge, UK: Cambridge University Press)
- Wittkowski, M., Hummel, C. A., Johnston, K. J., et al. 2001, A&A, 377, 981. doi:10.1051/0004-6361:20011124
- Wittkowski, M., Chiavassa, A., Freytag, B., et al. 2016, A&A, 587, A12.
doi:10.1051/0004-6361/201527614
- Zhao, M., Monnier, J. D., Pedretti, E., et al. 2009, ApJ, 701, 209.
doi:10.1088/0004-637X/701/1/209
- Zorec, J., Cidale, L., Arias, M. L., et al. 2009, A&A, 501, 297.
doi:10.1051/0004-6361/200811147

Table 1. NPOI Baselines.

Telescope Pair	Length (m)
AC-AE	18.9
AC-AN	22.8
AC-AW	22.2
AC-E3	9.8
AC-E6	34.4
AC-W4	8.8
AC-W7	51.3
AE-AN	34.9
AE-AW	37.5
AE-E6	15.9
AE-W4	26.7
AE-W7	64.2
AN-AW	38.2
AN-W7	66.4
AW-E3	31.9
AW-E6	53.3
AW-W4	14.0
AW-W7	29.5
E3-W4	18.6
E6-W4	42.5
E6-W7	79.4

Table 2. Sample Star Properties.

HD	HR	FK5	Other	Spectral	V	Parallax	Ref	[Fe/H]	Ref
			Name	Type	(mag)	(mas)			
3712	168	21	α Cas	K0 III	2.23	14.09 ± 0.50	1	-0.10	5
12929	617	74	α Ari	K2 III	2.01	49.56 ± 0.25	2	-0.17	5
17361	824	-	39 Ari	K0.5 III	4.51	19.04 ± 0.13	1	0.11	5
17506	834	99	η Per	K3 I-II	3.77	3.27 ± 0.19	1	0.04	5
37160	1907	-	ϕ^0 Ori	G9.5 III	4.08	28.67 ± 0.19	1	-0.54	5
50778	2574	266	θ CMa	K3/4 III	4.07	12.07 ± 0.13	1	-0.27	5
54719	2697	-	τ Gem	K2 III	4.41	8.33 ± 0.16	1	0.13	5
62044	2973	-	σ Gem	K1 III	4.26	27.12 ± 0.31	1	-0.06	5
87837	3980	-	31 Leo	K3.5 III	4.37	11.02 ± 0.17	1	0.07	5
102647	4534	444	β Leo	A3 V	2.14	90.91 ± 0.52	2	0.07	5
102870	4540	445	β Vir	F9 V	3.61	91.50 ± 0.22	2	0.12	5
112185	4905	483	ϵ UMa	A1 III-IV	1.76	41.22 ± 1.84	3	0.00	5
114710	4983	492	β Com	F9.5 V	4.26	109.23 ± 0.72	4	0.06	6
119228	5154	3087	83 UMa	M2 III	4.66	5.60 ± 0.14	1	0.30	5
124850	5338	525	ι Vir	F7 III	4.08	45.40 ± 0.29	1	-0.07	5
126660	5404	531	θ Boo	F7 V	4.05	69.07 ± 0.16	1	-0.02	5
127762	5435	535	γ Boo	A7 IV	3.04	39.91 ± 0.26	1	-0.20	5
128167	5447	1380	σ Boo	F4 V	4.47	63.47 ± 0.12	1	-0.32	5
141004	5868	-	λ Ser	G0 V	4.43	83.92 ± 0.15	1	-0.02	5
142373	5914	1416	χ Her	F8 V	4.62	62.92 ± 0.21	2	-0.45	5
146051	6056	603	δ Oph	M0.5 III	2.73	20.41 ± 0.54	1	-0.04	5
173667	7061	703	110 Her	F5.5 IV-V	4.20	51.67 ± 0.12	1	-0.03	5
173764	7063	1489	β Sct	G4 II	4.22	4.85 ± 0.34	1	-0.16	5
180809	7314	724	θ Lyr	K0 II	4.37	4.20 ± 0.11	1	0.08	5
183912	7417	732	β Cyg A	K3 II+B9.5 V	3.09	8.98 ± 0.45	1	-0.08	5
184406	7429	1511	μ Aql	K3 III	4.45	29.41 ± 0.14	1	0.00	5
198149	7957	783	η Cep	K0 IV	3.42	70.10 ± 0.11	2	-0.11	5
202444	8130	-	τ Cyg	F2 IV	3.73	49.58 ± 0.46	3	-0.11	7
203280	8162	803	α Cep	A8 V	2.45	66.50 ± 0.11	2	0.14	7
205435	8252	1568	ρ Cyg	G8 III	4.01	25.94 ± 0.10	1	-0.15	5
221115	8923	885	70 Peg	G8 III	4.55	17.19 ± 0.42	1	0.04	5
222107	8961	890	λ And	G8 IV	3.82	38.57 ± 0.12	1	-0.46	5
224014	9045	899	ρ Cas	G2	4.51	-0.06 ± 0.09	1	-0.21	5

NOTE—Spectral types are from SIMBAD, V magnitudes are from Mermilliod (1991), parallaxes and [Fe/H] are from the following sources: 1. Gaia Collaboration (2022); 2. van Leeuwen (2007); 3. Gaia Collaboration et al. (2018); 4. Mamajek & Hillenbrand (2008); 5. Anderson & Francis (2012); 6. Chen et al. (2020); and 7. Gáspár et al. (2016).

Table 3. Observing Log.

Target	Calibrator	Date	Baselines Used [†]	# Scans	# Data Points
HD	HD	(UT)			
3712	3360	2021 Oct 16	AC-W4	1	75
		2021 Oct 20	AC-AE, AC-W4	5	280
		2021 Oct 23	AC-AE, AC-W4	3	84
	6961	2021 Oct 16	AC-W4	1	90
		2021 Oct 20	AC-AE, AC-W4	5	280
		2021 Oct 23	AC-AE, AC-W4	3	84
12929	14055	2021 Oct 28	AC-AE, AW-W4	2	56
		2021 Oct 16	AC-AW	1	75
		2021 Oct 20	AC-AE, AC-W4	5	280
	17573	2021 Oct 23	AC-AE, AC-W4	3	84
		2021 Oct 16	AC-W4	1	75
		2021 Oct 20	AC-AE, AC-W4	5	280
17361	17573	2021 Oct 23	AC-AE, AC-W4	2	84
		2021 Oct 28	AC-AE, AW-W4	2	56
	17573	1997 Nov 18	AC-AE, AC-AW, AE-AW	4	166
		1997 Nov 19	AC-AE, AC-AW, AE-AW	2	78

NOTE—See Table 1 for the baseline lengths. “# Scans” is the number of scans per baseline included in the fourth column. This table shows the information for several stars as an example; the full table is available on the electronic version of the *Astronomical Journal*.

Table 4. Calibrator Stars' SED Inputs and Resulting Angular Diameters.

	Spec	<i>U</i>	<i>B</i>	<i>V</i>	<i>R</i>	<i>I</i>	<i>J</i>	<i>H</i>	<i>K</i>	<i>T</i> _{eff}	log <i>g</i>			θ_{est}	
HD	Type	(mag)	(K)	(cm s ⁻²)	Ref	<i>E(B - V)</i>	Ref	(mas)							
886	B2 IV	1.75	2.61	2.83	2.88	3.06	3.50	3.64	3.77	21944	3.93	1	0.02	8	0.45±0.02
3360	B2 IV	2.62	3.47	3.66	3.74	3.92	4.14	4.25	4.25	22180	3.92	2	0.03	9	0.32±0.02
6961	A7 V	4.63	4.51	4.34	4.25	4.16	4.45	4.28	4.13	7762	3.80	3	0.00	10	0.58±0.03
11415	B3 V	2.62	3.22	3.37	3.40	3.53	3.86	3.93	3.96	14250	3.38	4	0.05	11	0.50±0.03
14055	A1 V	4.04	4.03	4.01	3.99	4.00	3.80	3.86	3.96	9333	4.19	3	0.02	9	0.56±0.03
17573	B8 V	3.16	3.51	3.61	3.64	3.73	3.66	3.80	3.86	11749	4.14	3	0.01	9	0.52±0.03
25642	A0 IV	4.23	4.27	4.29	4.27	4.30	4.08	4.15	4.15	10900	3.7	5	0.08	12	0.50±0.02
35468	B2 V	0.55	1.41	1.64	1.71	1.84	2.15	2.36	2.38	21380	3.81	3	0.02	11	0.82±0.04
37490	B3 V	3.72	4.48	4.58	4.56	4.67	5.01	4.92	4.81	17660	3.58	6	0.05	13	0.26±0.01
45725	B4 V	3.87	4.50	4.60	4.69	4.82	3.72	3.52	4.08	21135	4.00	6	0.04	11	0.30±0.01
50019	A2 IV	3.84	3.70	3.60	3.53	3.48	3.25	3.23	3.16	8128	3.50	3	0.03	12	0.83±0.04
58142	A0.5 V	4.59	4.60	4.62	4.62	4.65	4.70	4.69	4.57	9333	3.82	3	0.02	12	0.41±0.02
91316	B1 I	2.76	3.71	3.85	3.89	4.03	4.27	4.26	4.28	24200	3.09	7	0.04	14	0.28±0.01
97633	A2 IV	3.37	3.33	3.34	3.29	3.30	3.12	3.19	3.08	9120	3.62	3	0.01	8	0.78±0.04
98664	B9.5 V	3.89	3.99	4.04	4.07	4.13	4.37	4.33	4.14	10233	3.89	3	0.02	9	0.48±0.02
106591	A2 V	3.46	3.39	3.31	3.24	3.21	3.32	3.31	3.10	8710	4.12	3	0.00	12	0.81±0.04
112413	A0 V	2.45	2.78	2.89	2.88	2.94	3.06	3.13	3.15	12589	4.23	3	0.01	8	0.67±0.03
118098	A2 V	3.60	3.49	3.37	3.31	3.25	3.26	3.15	3.22	8511	4.19	3	0.02	15	0.83±0.04
122408	A2 IV/V	4.48	4.36	4.25	4.19	4.14	4.21	4.11	4.09	8128	3.58	3	0.11	16	0.64±0.03
124675	A7 IV	4.86	4.72	4.52	4.42	4.33	4.21	4.16	4.10	7586	3.75	3	0.02	12	0.58±0.03
125162	A0 V	4.32	4.26	4.18	4.13	4.10	3.98	4.03	3.91	8710	4.26	3	0.01	17	0.56±0.03
130109	A0 III	3.71	3.73	3.74	3.72	3.74	3.68	3.63	3.65	9550	4.07	3	0.01	12	0.59±0.03
135742	B8 V	2.14	2.51	2.61	2.60	2.67	2.76	2.89	2.91	10233	3.61	3	0.02	9	0.95±0.05
141003	A2 IV	3.82	3.73	3.67	3.60	3.57	3.44	3.54	3.55	8511	3.69	3	0.02	9	0.73±0.04
141513	B9.5 III	3.42	3.50	3.54	3.56	3.60	3.80	3.76	3.70	9772	3.88	3	0.02	12	0.63±0.03
141795	A7 V	3.99	3.86	3.71	3.63	3.56	3.56	3.44	3.43	8318	4.26	3	0.00	18	0.72±0.04
147394	B5 IV	3.19	3.74	3.90	3.94	4.07	3.93	4.09	4.29	14791	3.98	3	0.03	9	0.38±0.02
149757	O9.2 IV	1.72	2.58	2.57	2.53	2.53	2.53	2.67	2.68	29242	4.00	6	0.31	11	0.57±0.03
176437	B9 III	3.10	3.20	3.25	3.24	3.28	3.12	3.23	3.12	10080	3.50	6	0.02	8	0.74±0.04
177756	B8.5 V	3.07	3.34	3.43	3.44	3.52	3.52	3.48	3.56	11749	4.22	3	0.00	19	0.56±0.03
184006	A5 V	4.07	3.93	3.78	3.69	3.62	3.74	3.69	3.60	7943	3.77	3	0.00	12	0.76±0.04
184930	B5 III	3.84	4.28	4.36	4.37	4.46	4.44	4.42	4.48	10471	3.72	3	0.14	15	0.45±0.02
202850	A0 I	3.97	4.36	4.23	4.20	4.17	3.97	3.86	3.68	10388	1.80	6	0.20	9	0.55±0.03
210459	F5 III	4.93	4.75	4.29	4.01	3.78	3.49	3.30	3.12	6457	3.09	3	0.00	10	0.90±0.04
213558	A1 V	3.78	3.77	3.76	3.75	3.76	3.83	3.87	3.85	9333	4.20	3	0.00	19	0.60±0.03
214923	B8 V	3.10	3.32	3.41	3.43	3.51	3.54	3.53	3.57	10965	3.75	3	0.01	9	0.60±0.03

NOTE—Spectral types are from SIMBAD; *UBV* values are from Mermilliod (1991); *RI* values are from Monet et al. (2003); *JHK* values are from Cutri et al. (2003); *T*_{eff}, log *g*, and *E(B - V)* values are from the following sources: 1. Prugniel et al. (2007); 2. Valdes et al. (2004); 3. Allende Prieto & Lambert (1999); 4. Huang et al. (2010); 5. Gebran et al. (2016); 6. Soubiran et al. (2016); 7. Le Borgne et al. (2003); 8. Sánchez-Blázquez et al. (2006); 9. Zorec et al. (2009); 10. Clem et al. (2004); 11. Friedemann (1992); 12. Neckel et al. (1980); 13. Hunter et al. (2006); 14. Jenkins (2009); 15. Gontcharov & Mosenkov (2018); 16. van Belle et al. (2008); 17. Otte & Dixon (2006); 18. Koleva & Vazdekis (2012); and 19. Alonso et al. (1996). θ_{est} is the estimated angular diameter calculated using the method described in Section 3.

Table 5. Interferometric Results.

Target	θ_{UD}	T_{eff}	$\log g$	Initial	$\theta_{LD,\text{initial}}$	Final	$\theta_{LD,\text{final}}$	σ_{LD}	Max SF	#	#
HD	(mas)	(K)	(cm s $^{-2}$)	μ_λ	(mas)	μ_λ	(mas)	(%)	(10 6 cycles rad $^{-1}$)	scans	pts
3712	5.519±0.002	4690	1.19	0.67	5.871±0.036	0.71	5.903±0.036	0.6	33.6	9	949
12929	6.531±0.002	4439	2.00	0.70	6.975±0.027	0.73	7.006±0.027	0.4	33.7	11	934
17361	1.692±0.017	4724	2.40	0.69	1.810±0.127	0.69	1.810±0.127	7.0	63.8	6	244
17506	4.760±0.005	3924	0.26	0.78	5.260±0.073	0.78	5.260±0.073	1.4	29.3	5	520
37160	1.948±0.001	4855	2.61	0.64	2.188±0.010	0.66	2.193±0.010	0.5	81.1	56	2799
50778	3.693±0.006	4062	1.36	0.76	3.725±0.074	0.73	3.707±0.074	2.0	82.2	8	208
54719	2.348±0.011	7799	1.64	0.71	2.346±0.071	0.71	2.346±0.069	2.9	117.6	6	102
62044	2.175±0.002	4591	2.48	0.71	2.266±0.030	0.69	2.260±0.030	1.3	67.8	12	519
87837	3.344±0.008	4121	1.42	0.76	3.464±0.048	0.78	3.476±0.048	1.4	138.2	6	345
102647	1.422±0.001	8730	4.28	0.44	1.479±0.013	0.46	1.482±0.013	0.9	94.8	58	2981
102870	1.687±0.005	6171	4.06	0.54	1.754±0.069	0.61	1.768±0.070	4.0	39.6	68	1322
112185	1.587±0.001	9760	3.59	0.41	1.641±0.020	0.43	1.644±0.020	1.2	71.1	7	362
114710	0.856±0.013	6061	4.43	0.56	0.891±0.171	0.52	0.887±0.171	19.3	39.6	72	1296
119228	4.068±0.010	3678	0.54	0.82	4.376±0.117	0.76	4.338±0.117	2.7	27.9	16	280
124850	1.164±0.005	6201	3.65	0.52	1.219±0.061	0.54	1.222±0.061	5.0	64.6	29	929
126660	0.841±0.007	6355	4.08	0.53	0.906±0.097	0.49	0.902±0.097	10.8	40.2	104	2136
127762	1.697±0.001	7793	3.63	0.50	1.722±0.011	0.52	1.726±0.011	0.6	67.3	43	2981
128167	0.613±0.019	6749	4.32	0.50	0.715±0.205	0.48	0.714±0.205	28.7	36.4	69	1254
141004	0.908±0.004	5981	4.22	0.55	0.982±0.056	0.55	0.982±0.056	5.7	64.6	247	5685
142373	0.963±0.012	5577	3.81	0.57	1.053±0.143	0.56	1.051±0.143	13.6	33.8	84	1600
146051	9.365±0.002	3811	0.94	0.81	10.144±0.020	0.82	10.161±0.020	0.2	28.5	47	1260
173667	0.859±0.002	6605	4.01	0.50	0.904±0.022	0.51	0.905±0.022	2.4	98.6	37	1932
173764	2.121±0.001	4748	0.78	0.67	2.235±0.011	0.63	2.223±0.011	0.5	121.0	146	6529
180809	2.231±0.003	4507	0.79	0.71	2.357±0.045	0.71	2.357±0.045	1.9	61.1	14	479
183912	4.596±0.003	4477	0.84	0.70	4.924±0.035	0.67	4.904±0.035	0.7	38.5	75	1635
184406	1.922±0.004	4475	2.58	0.71	2.040±0.040	0.68	2.032±0.040	2.0	91.8	5	278
198149	2.389±0.001	5057	3.27	0.65	2.518±0.009	0.65	2.518±0.009	0.4	71.0	60	2118
202444	2.013±0.002	6214	3.62	0.52	2.128±0.027	0.68	2.169±0.028	1.3	49.2	283	5847
203280	1.597±0.001	7806	3.90	0.46	1.674±0.008	0.48	1.677±0.007	0.4	71.1	146	5715
205435	1.903±0.001	5133	2.66	0.63	1.967±0.035	0.67	1.977±0.036	1.8	71.0	14	548
221115	1.356±0.013	5062	2.57	0.65	1.434±0.104	0.64	1.432±0.104	7.3	63.4	13	538
222107	2.634±0.001	4667	2.69	0.68	2.769±0.012	0.69	2.772±0.012	0.4	71.1	39	1660
224014*	2.454±0.004	3846	4.72	0.63	2.562±0.042	0.63	2.562±0.043	1.7	67.1	10	393

NOTE—The initial μ_λ is based on the T_{eff} and $\log g$ listed here, and the final μ_λ is based on the new T_{eff} determination (see Section 4 for more details). The T_{eff} and $\log g$ are from McDonald et al. (2017) except for HD 224014, which is from Robin et al. (2012). Max SF is the maximum spatial frequency for that star’s diameter measurement, # scans is the total number of scans used, and # pts is the number of data points in the angular diameter fit.

*The diameter fit for this target may not be of significant value without knowledge of the pulsation phase of the star, as described in Section 5.

Table 6. Photometry & Spectrophotometry Sources.

Reference	System
Mendoza (1967)	Johnson <i>UBVRI</i>
Johnson (1963)	<i>IJHKLMN</i>
Kakaras et al. (1968)	<i>UPXYZVS</i>
Häggkvist & Oja (1970)	Oja
Golay (1972)	Geneva <i>VBUB₁B₂V₁G</i>
Johnson & Mitchell (1975)	13 color photometry
Morel & Magnenat (1978)	<i>UBVRIJKLMNH</i>
Alexander et al. (1983)	m746, m608, m683, m710
Burnashev (1985)	Spectrophotometry
Mermilliod (1987)	Johnson <i>UBV</i>
Helou & Walker (1988)	IRAS fluxes
Kharitonov et al. (1988)	Spectrophotometry
Mermilliod & Nitschelm (1989)	DDO
Kornilov et al. (1991)	<i>WBVR</i>
Gezari et al. (1993)	Catalog of Infrared Observations
Straizys et al. (1995)	Vilnius <i>UPXYZVS</i>
Alekseeva et al. (1997)	Spectrophotometry
Glushneva et al. (1998)	Spectrophotometry
Gezari et al. (1999)	Catalog of Infrared Observations
Hög et al. (2000)	Tycho <i>B_tV_t</i>
Ducati (2002)	Johnson <i>UBV</i> , Cousins <i>R_cI_c</i>
Cutri et al. (2003)	2MASS <i>JHK</i>
Smith et al. (2004)	COBE Point Source Catalog
van Leeuwen (2007)	Hipparcos <i>H_p</i>

NOTE—These are the sources used in the SED fitting procedure described in Section 4.

Table 7. Derived Stellar Parameters.

Target	Spectral	R	σ_R	F_{BOL}	A_V	T_{eff}	σ_T	L
HD	Type	(R_\odot)	(%)	(10^{-6} erg s $^{-1}$ cm $^{-2}$)	(mag)	(K)	(%)	(L_\odot)
3712	K2 III-IV	45.03 $\pm^{1.57}_{1.68}$	3.6	4.66 ± 0.022	0.02 ± 0.01	4476 ± 15	0.3	734.2 ± 52.2
12929	K2.5 III-IV	15.19 ± 0.10	0.6	5.98 ± 0.004	0.00 ± 0.00	4373 ± 8	0.2	76.2 ± 0.8
17361	K2.5 IV	10.22 ± 0.72	7.1	0.56 ± 0.002	0.00 ± 0.00	4768 ± 167	3.5	48.7 ± 0.7
17506	K3.5 I-II	173.10 $\pm^{9.69}_{10.80}$	6.2	2.56 ± 0.022	0.47 ± 0.01	4082 ± 30	0.7	7508 ± 864
37160	G8 III	8.22 ± 0.07	0.8	0.78 ± 0.001	0.00 ± 0.00	4703 ± 11	0.2	29.8 ± 0.4
50778	K5 III-IV	33.01 ± 0.75	2.3	1.42 ± 0.011	0.11 ± 0.01	4196 ± 43	1.0	304.9 ± 7.0
54719	K3 IV	30.27 $\pm^{1.08}_{1.09}$	3.6	0.81 ± 0.007	0.31 ± 0.01	4583 ± 70	1.5	364.7 ± 14.4
62044	K2.5 IV	8.96 ± 0.16	1.8	0.78 ± 0.001	0.00 ± 0.00	4627 ± 31	0.7	33.2 ± 0.8
87837	K5 III-IV	33.90 $\pm^{0.70}_{0.71}$	2.1	1.10 ± 0.009	0.12 ± 0.01	4066 ± 29	0.7	283.3 ± 9.0
102647	A4 IV-V	1.75 ± 0.02	1.0	3.41 ± 0.003	0.00 ± 0.00	8262 ± 36	0.4	12.9 ± 0.1
102870	F8 IV-V	2.08 ± 0.08	4.0	0.92 ± 0.000	0.00 ± 0.00	5456 ± 108	2.0	3.4 ± 0.0
112185	A0 IV	4.29 ± 0.19	4.8	0.00 ± 0.000	0.00 ± 0.00	8908 ± 54	0.6	104.4 ± 9.3
114710	F9 IV-V	0.87 ± 0.17	19.3	0.50 ± 0.001	0.00 ± 0.00	6612 ± 637	9.6	1.3 ± 0.0
119228	K6 I-II	83.31 $\pm^{3.03}_{3.10}$	3.7	1.61 ± 0.023	0.39 ± 0.01	4003 ± 56	1.4	1608 ± 84
124850	F6 V	2.89 ± 0.15	5.0	0.67 ± 0.001	0.00 ± 0.00	6055 ± 151	2.5	10.2 ± 0.1
126660	F6 V	1.40 ± 0.15	10.8	0.61 ± 0.000	0.00 ± 0.00	6885 ± 370	5.4	4.0 ± 0.0
127762	A6 V	4.65 ± 0.04	0.9	1.47 ± 0.001	0.00 ± 0.00	6203 ± 20	0.3	28.9 ± 0.4
128167	F3 IV	1.21 ± 0.35	28.7	0.39 ± 0.000	0.00 ± 0.00	6922 ± 994	14.4	3.0 ± 0.0
141004	G1 V	1.26 ± 0.07	5.7	0.44 ± 0.000	0.00 ± 0.00	6087 ± 174	2.9	2.0 ± 0.0
142373	F8 V	1.80 ± 0.24	13.6	0.38 ± 0.000	0.00 ± 0.00	5668 ± 386	6.8	3.0 ± 0.0
146051	K4.5 I-II	53.50 $\pm^{1.38}_{1.46}$	2.7	6.68 ± 0.020	0.20 ± 0.00	3733 ± 5	0.1	501.6 ± 26.6
173667	F5 V	1.88 ± 0.05	2.4	0.51 ± 0.001	0.00 ± 0.00	6568 ± 80	1.2	6.0 ± 0.0
173764	G4 I-II	49.26 $\pm^{3.24}_{3.72}$	7.6	0.99 ± 0.017	0.65 ± 0.01	4951 ± 25	0.5	1315 ± 186
180809	K2 II-III	60.31 $\pm^{1.92}_{1.99}$	3.3	0.78 ± 0.005	0.07 ± 0.01	4523 ± 44	1.0	1374 ± 73
183912	G3 II	58.69 $\pm^{2.83}_{3.12}$	5.3	4.47 ± 0.038	1.11 ± 0.00	4860 ± 20	0.4	1734 ± 174
184406	K2.5 III	7.43 ± 0.15	2.0	0.70 ± 0.001	0.00 ± 0.00	4746 ± 47	1.0	25.2 ± 0.2
198149	G9 III-IV	3.86 ± 0.02	0.4	1.32 ± 0.001	0.00 ± 0.00	5000 ± 9	0.2	8.4 ± 0.0
202444	F4 III-IV	4.70 ± 0.07	1.6	0.81 ± 0.002	0.00 ± 0.00	4771 ± 31	0.6	10.3 ± 0.2
203280	A8 III-IV	2.71 ± 0.01	0.4	2.45 ± 0.002	0.00 ± 0.00	7151 ± 15	0.2	17.3 ± 0.1
205435	G3 I-II	8.19 ± 0.15	1.9	0.67 ± 0.001	0.00 ± 0.00	4770 ± 43	0.9	31.3 ± 0.2
221115	G7 II-III	8.95 ± 0.69	7.7	0.47 ± 0.001	0.00 ± 0.00	5108 ± 185	3.6	49.2 ± 2.4
222107	K2.5 IV-V	7.72 ± 0.04	0.5	1.08 ± 0.001	0.00 ± 0.00	4532 ± 10	0.2	22.7 ± 0.1

NOTE—The spectral types are those that provide the best SED fit as described in Section 4. The SED fits are also the source of F_{BOL} and A_V . The other parameters are derived as described in Section 4.

Table 8. Comparing NPOI Diameters to Previous Measurements.

Target	θ_{LD} , here		Reference
	HD	(mas)	
3712	5.903 \pm 0.036	5.4 \pm 0.6	Bonneau et al. (1981)
		5.4 \pm 0.6	Faucherre et al. (1983)
		5.64 \pm 0.05	Mozurkewich et al. (1991)
		5.60 \pm 0.06	Nordgren et al. (1999)
		5.72 \pm 0.08	Nordgren et al. (2001)
		5.65 \pm 0.08	Nordgren et al. (2001)
		5.608 \pm 0.056	Mozurkewich et al. (2003)
12929	7.006 \pm 0.027	7.6 \pm 1.0	Faucherre et al. (1983)
		6.848 \pm 0.07	Mozurkewich et al. (1991)
		5.9 \pm 0.6*	Dyck et al. (1998)
		6.88 \pm 0.04	Nordgren et al. (1999)
		6.84 \pm 0.10	Nordgren et al. (2001)
		6.94 \pm 0.08	Nordgren et al. (2001)
		6.827 \pm 0.068	Mozurkewich et al. (2003)
17361	1.810 \pm 0.127	6.792 \pm 0.043	Hutter et al. (2016)
		1.88 \pm 0.11	Nordgren et al. (1999)
		5.381 \pm 0.055	Mozurkewich et al. (2003)
		2.169 \pm 0.010	Richichi & Percheron (2005)
		3.707 \pm 0.074	Richichi & Percheron (2005)
		4.13 \pm 0.40*	Cruzelèbes et al. (2019)
		3.904 \pm 0.015	Cruzelèbes et al. (2019)
17506	5.260 \pm 0.073	2.346 \pm 0.069	Cruzelèbes et al. (2019)
		2.356 \pm 0.012	Cruzelèbes et al. (2019)
		2.260 \pm 0.030	Nordgren et al. (1999)
		2.417 \pm 0.007	Roettenbacher et al. (2015)
		3.476 \pm 0.048	Nordgren et al. (1999)
		3.33 \pm 0.04	Richichi & Percheron (2005)
		3.276 \pm 0.014	Cruzelèbes et al. (2019)
37160	2.169 \pm 0.010	1.482 \pm 0.013	1.25 \pm 0.09*
			Hanbury Brown et al. (1974b)
			Di Folco et al. (2004)
			Akeson et al. (2009)
50778	3.707 \pm 0.074		1.388 \pm 0.049
			van Belle & von Braun (2009)
			Boyajian et al. (2012b)
			N/A
54719	2.346 \pm 0.069	1.644 \pm 0.020	1.071 \pm 0.057
			van Belle & von Braun (2009)
62044	2.260 \pm 0.030	0.887 \pm 0.171	1.127 \pm 0.011
			Boyajian et al. (2012b)
87837	3.476 \pm 0.048	1.768 \pm 0.070	4.338 \pm 0.117
			N/A
102647	1.482 \pm 0.013	1.644 \pm 0.020	1.222 \pm 0.061
			1.222 \pm 0.061
102870	1.768 \pm 0.070	0.902 \pm 0.097	0.902 \pm 0.097
			1.130 \pm 0.055
112185	1.644 \pm 0.020	0.887 \pm 0.171	0.841 \pm 0.013
			0.841 \pm 0.013
114710	0.887 \pm 0.171	1.071 \pm 0.057	0.982 \pm 0.056
			0.838 \pm 0.120
119228	4.338 \pm 0.117	1.127 \pm 0.011	1.051 \pm 0.143
			N/A
124850	1.222 \pm 0.061	1.109 \pm 0.007	1.051 \pm 0.143
			N/A
126660	0.902 \pm 0.097	1.109 \pm 0.007	1.051 \pm 0.143
			N/A
127762	1.726 \pm 0.011	0.841 \pm 0.013	0.714 \pm 0.205
			0.841 \pm 0.013
128167	0.714 \pm 0.205	0.838 \pm 0.120	0.982 \pm 0.056
			0.838 \pm 0.120
141004	0.982 \pm 0.056	1.051 \pm 0.143	1.051 \pm 0.143
			N/A
142373	1.051 \pm 0.143		1.051 \pm 0.143
			N/A

Table 8 continued on next page

Table 8 (*continued*)

Target	$\theta_{\text{LD,here}}$		Reference
	HD	(mas)	
146051	10.161 \pm 0.020	9.3 \pm 0.5*	Dyck et al. (1996)
		10.08 \pm 0.48*	Perrin et al. (1998)
		9.3 \pm 0.4*	Dyck et al. (1998)
		10.471 \pm 0.117	Mozurkewich et al. (2003)
		9.60 \pm 0.37*	Richichi & Percheron (2005)
173667	0.905 \pm 0.022	9.93 \pm 0.09	Cruzalèbes et al. (2013)
		1.000 \pm 0.006	Boyajian et al. (2012b)
		N/A	
173764	2.223 \pm 0.011	2.23 \pm 0.09	Nordgren et al. (1999)
		2.373 \pm 0.009	van Belle et al. (2009)
180809	2.357 \pm 0.045	4.834 \pm 0.048	Mozurkewich et al. (2003)
183912	4.904 \pm 0.035	2.149 \pm 0.010	Cruzalèbes et al. (2019)
184406	2.032 \pm 0.040	2.65 \pm 0.04	Nordgren et al. (1999)
		2.882 \pm 0.088	Hutter et al. (2016)
198149	2.518 \pm 0.009	N/A	
202444	2.169 \pm 0.028	2.759 \pm 0.050	Parks et al. (2021)
		2.742 \pm 0.010	Martinez et al. (2021)
203280	1.677 \pm 0.007	2.47 \pm 0.05	Nordgren et al. (1999)
		2.151 \pm 0.038	van Belle et al. (2009)
205435	1.977 \pm 0.036	1.82 \pm 0.10	Nordgren et al. (1999)
221115	1.432 \pm 0.104	1.61 \pm 0.17	Nordgren et al. (1999)
222107	2.772 \pm 0.012	2.66 \pm 0.08	Nordgren et al. (1999)
		2.759 \pm 0.050	Parks et al. (2021)
		2.742 \pm 0.010	Martinez et al. (2021)
224014	2.562 \pm 0.043	2.47 \pm 0.05	Nordgren et al. (1999)
		2.151 \pm 0.038	van Belle et al. (2009)

NOTE—*No LD diameter was provided, so we list the UD diameter here. Figure 3 shows a graphical representation of this table. If more than one diameter was available in the literature, we used the most recent one when plotting the results.

Table 9. Current and Previous NPOI Diameters as an Ensemble.

Target	$\theta_{LD,NPOI}$		<i>V</i>	A_V	<i>K</i>	$\theta_{LD,Mozur}$	$\theta_{LD,Adams}$	Star	$\theta_{LD,JMMC}$	$\theta_{LD,Gaia}$
	HD	(mas)	Ref	(mag)	(mag)	(mag)	(mas)	(mas)	in range?	(mas)
432	2.103±0.015	1	2.27±0.01	0.06	1.45±0.20	1.98±0.41	2.04±0.07	N	1.967±0.245	1.976
1013	4.359±0.022	1	4.80±0.01	0.12	0.72±0.21	4.22±0.82	4.16±0.15	N	4.404±0.342	3.873
1522	3.310±0.062	1	3.54±0.02	0.17	1.03±0.27	3.05±0.83	3.00±0.11	Y	3.159±0.283	3.552
3627	4.185±0.036	2	3.27±0.03	0.10	0.47±0.19	4.13±0.75	4.04±0.15	Y	4.529±0.368	4.154
3712	5.903±0.036	3	2.23±0.01	0.14	-0.30±0.17	5.65±0.82	5.55±0.20	Y	5.789±0.394	0.278
4656	3.841±0.035	2	4.43±0.01	0.15	1.11±0.17	3.25±0.56	3.18±0.11	Y	3.273±0.314	3.395
5112	3.730±0.041	2	4.76±0.01	0.16	1.02±0.30	3.55±1.02	3.48±0.13	Y	3.560±0.357	3.576
6186	1.887±0.025	4	4.27±0.01	0.11	2.12±0.27	1.77±0.43	1.75±0.06	Y	1.809±0.176	2.009
6805	3.304±0.012	2	3.44±0.01	0.10	0.92±0.25	3.23±0.82	3.17±0.11	Y	3.274±0.312	3.391
8512	2.764±0.016	1	3.60±0.01	0.09	1.29±0.30	2.66±0.82	2.62±0.09	Y	2.708±0.313	3.095
9826	1.083±0.018	2	4.09±0.01	0.05	2.86±0.27	1.11±0.08	1.12±0.04	N	1.118±0.137	1.186
9927	3.649±0.007	1	3.57±0.01	0.14	0.65±0.20	3.83±0.76	3.75±0.14	Y	3.931±0.322	3.798
10380	2.873±0.045	2	4.44±0.01	0.10	1.36±0.31	2.83±0.88	2.77±0.10	Y	2.808±0.289	3.071
10700	2.072±0.010	5	3.50±0.01	0.00	1.79±0.27	1.96±0.53	1.95±0.06	Y	N/A	2.220
10761	1.677±0.018	4	4.26±0.01	0.08	2.03±0.26	1.87±0.45	1.85±0.07	Y	1.884±0.163	1.840
12929	7.006±0.027	3	2.01±0.01	0.07	-0.78±0.18	7.36±0.97	7.20±0.26	Y	7.620±0.566	7.325
17361	1.810±0.127	3	4.51±0.01	0.16	2.10±0.28	1.84±0.47	1.81±0.07	Y	1.818±0.196	1.999
17506	5.260±0.073	3	3.77±0.02	0.44	0.16±0.17	5.02±0.75	4.91±0.18	Y	5.242±0.399	4.027
17709	3.907±0.021	1	4.54±0.01	0.25	0.77±0.18	3.96±0.67	3.87±0.14	Y	4.140±0.378	4.066
18925	3.894±0.018	1	2.93±0.01	0.16	1.09±0.20	2.71±0.57	2.70±0.10	N	2.904±0.252	4.574
19373	1.017±0.031	2	4.05±0.01	0.00	2.72±0.27	1.21±0.14	1.22±0.04	N	1.171±0.155	1.275
20644	3.674±0.025	1	4.47±0.01	0.37	0.88±0.17	3.64±0.60	3.55±0.13	Y	3.881±0.347	3.804
20902	3.180±0.008	2	1.80±0.01	0.35	0.52±0.16	3.13±0.55	3.20±0.12	N	3.347±0.215	3.276
25025	9.286±0.028	2	2.95±0.01	0.13	-0.95±0.23	8.97±1.32	8.81±0.32	Y	9.149±0.727	9.909
28305	2.592±0.050	1	3.54±0.01	0.17	1.42±0.25	2.40±0.63	2.38±0.09	Y	2.727±0.260	3.146
28307	2.172±0.033	2	3.84±0.01	0.17	1.64±0.22	2.20±0.48	2.17±0.08	Y	2.288±0.179	2.267
31964	2.210±0.012	1	2.98±0.02	1.15	1.53±0.21	1.77±0.37	1.87±0.07	N	1.948±0.195	N/A
34085	2.606±0.009	1	0.14±0.03	0.24	0.21±0.40	2.91±1.29	3.19±0.11	N	2.721±0.360	3.104
35497	1.239±0.052	2	1.65±0.01	0.18	2.00±0.24	1.23±0.15	1.36±0.05	Y	1.155±0.973	1.001
37160	2.193±0.010	3	4.08±0.01	0.17	1.81±0.23	2.06±0.47	2.03±0.07	Y	2.152±0.188	2.358
38944	4.310±0.036	1	4.74±0.01	0.34	0.68±0.19	4.21±0.73	4.13±0.15	Y	4.365±0.473	3.712
39003	2.681±0.027	2	3.96±0.01	0.19	1.52±0.20	2.39±0.50	2.36±0.08	Y	2.418±0.267	2.687
42995	12.112±0.024	2	3.28±0.01	0.23	-1.72±0.15	14.07±1.02	14.14±0.51	N	N/A	6.335
43232	3.097±0.034	1	3.97±0.01	0.28	1.09±0.25	3.06±0.76	3.00±0.11	Y	3.124±0.373	3.930
48329	4.677±0.013	1	2.99±0.01	0.27	0.13±0.17	4.76±0.75	4.67±0.17	Y	4.709±0.356	7.108
50778	3.707±0.074	3	4.07±0.01	0.36	0.64±0.26	3.98±1.00	3.89±0.14	Y	4.055±0.386	4.033
54719	2.346±0.069	3	4.41±0.01	0.16	1.68±0.25	2.32±0.59	2.27±0.08	Y	2.370±0.247	2.575
58207	2.390±0.024	1	3.79±0.01	0.13	1.56±0.18	2.30±0.42	2.27±0.08	Y	2.335±0.234	2.716
60522	4.748±0.030	2	4.06±0.01	0.17	0.23±0.21	5.14±0.91	5.04±0.18	Y	5.631±0.457	4.677
61421	5.406±0.006	2	0.37±0.01	0.00	-0.66±0.32	5.46±1.59	5.57±0.20	N	5.665±0.613	N/A
61935	2.170±0.021	2	3.93±0.01	0.27	1.64±0.31	2.19±0.69	2.17±0.08	Y	2.319±0.241	2.527
62044	2.260±0.030	3	4.26±0.03	0.12	1.74±0.20	2.21±0.45	2.17±0.07	Y	2.301±0.245	2.576
62345	2.361±0.025	1	3.57±0.01	0.15	1.53±0.26	2.27±0.61	2.25±0.08	Y	2.337±0.248	2.926
62509	8.134±0.013	1	1.14±0.01	0.03	-0.94±0.16	7.23±0.89	7.14±0.26	Y	7.390±0.581	N/A

Table 9 continued on next page

Table 9 (*continued*)

Target	$\theta_{LD,NPOI}$		V	A_V	K	$\theta_{LD,Mozur}$	$\theta_{LD,Adams}$	Star	$\theta_{LD,JMMC}$	$\theta_{LD,Gaia}$
HD	(mas)	Ref	(mag)	(mag)	(mag)	(mas)	(mas)	in range?	(mas)	(mas)
66141	2.747±0.039	1	4.39±0.01	0.33	1.45±0.31	2.60±0.81	2.55±0.09	Y	2.691±0.277	2.852
69267	5.167±0.035	1	3.53±0.01	0.23	0.19±0.20	4.92±0.88	4.81±0.17	Y	4.943±0.418	4.636
70272	4.228±0.024	1	4.25±0.01	0.11	0.38±0.18	4.86±0.75	4.77±0.17	N	4.891±0.487	4.524
74442	2.595±0.021	2	3.94±0.01	0.12	1.57±0.20	2.34±0.49	2.31±0.08	Y	2.381±0.234	2.669
76294	3.196±0.017	1	3.11±0.01	0.19	0.70±0.19	3.49±0.67	3.43±0.12	Y	3.522±0.279	3.411
80493	7.954±0.027	2	3.14±0.01	0.09	-0.66±0.17	7.77±0.94	7.63±0.27	Y	8.216±0.616	7.143
82308	4.143±0.025	1	4.31±0.01	0.15	0.59±0.20	4.33±0.80	4.24±0.15	Y	4.463±0.421	4.462
82328	1.662±0.013	1	3.18±0.01	0.03	1.97±0.25	1.67±0.37	1.69±0.06	N	1.653±0.159	1.542
83618	3.462±0.033	1	3.90±0.01	0.20	0.87±0.26	3.47±0.89	3.40±0.12	Y	3.521±0.345	4.068
84441	2.587±0.025	1	2.98±0.01	0.13	1.22±0.23	2.52±0.60	2.51±0.09	N	2.657±0.236	2.174
85503	2.887±0.016	1	3.88±0.01	0.05	1.36±0.22	2.65±0.61	2.60±0.09	Y	2.815±0.227	3.149
87837	3.476±0.048	3	4.37±0.01	0.15	1.02±0.32	3.39±1.07	3.32±0.10	Y	3.372±0.362	3.641
87901	1.664±0.037	1	1.36±0.01	0.06	1.64±0.21	1.50±0.26	1.65±0.06	N	1.353±0.144	1.305
89758	8.579±0.029	2	3.05±0.01	0.06	-1.01±0.17	9.42±1.01	9.29±0.33	N	9.950±0.658	6.260
94264	2.626±0.009	1	3.82±0.02	0.02	1.53±0.19	2.39±0.47	2.35±0.08	Y	N/A	2.727
95689	6.419±0.041	1	1.80±0.01	0.03	-0.83±0.17	7.39±0.94	7.25±0.26	Y	N/A	7.127
96833	4.131±0.007	1	3.01±0.01	0.00	0.43±0.20	4.13±0.78	4.05±0.15	Y	4.323±0.294	3.829
97778	6.182±0.057	1	4.63±0.01	0.24	-0.07±0.20	6.40±0.96	6.38±0.23	N	6.583±0.519	5.897
98262	4.561±0.016	1	3.48±0.01	0.12	0.28±0.18	4.70±0.77	4.60±0.17	Y	4.949±0.324	4.554
100029	6.376±0.012	1	3.85±0.02	0.11	-0.11±0.17	6.15±0.84	6.04±0.22	Y	6.427±0.465	4.487
102212	5.657±0.013	1	4.03±0.01	0.07	0.16±0.26	5.40±1.17	5.31±0.19	Y	5.557±0.487	4.872
102224	3.541±0.022	2	3.71±0.01	0.02	0.99±0.19	3.25±0.62	3.18±0.11	Y	3.260±0.287	3.602
102647	1.482±0.013	3	2.14±0.01	0.02	1.88±0.19	1.49±0.23	1.57±0.05	Y	1.471±0.137	1.361
102870	1.768±0.070	3	3.61±0.01	0.02	2.27±0.25	1.49±0.29	1.50±0.04	Y	1.477±0.127	1.506
108381	2.179±0.057	1	4.35±0.01	0.00	1.81±0.25	2.18±0.54	2.14±0.08	Y	2.083±0.176	1.985
108907	5.420±0.010	1	4.96±0.00	0.11	0.45±0.17	5.00±0.71	4.97±0.18	N	5.231±0.462	4.439
109358	1.133±0.034	1	4.26±0.01	0.01	2.85±0.31	1.15±0.13	1.16±0.04	N	1.148±0.120	1.145
109387	0.906±0.049	2	3.85±0.03	0.10	3.82±0.04	0.58±0.08	0.62±0.02	N	0.467±0.423	0.984
112185	1.644±0.020	3	1.76±0.01	0.03	1.63±0.27	1.64±0.40	1.75±0.05	Y	1.526±0.139	1.472
112300	10.918±0.021	2	3.38±0.01	0.01	-1.19±0.19	10.80±1.20	10.78±0.39	N	11.024±0.736	8.568
113226	3.318±0.013	1	2.83±0.02	0.03	0.66±0.28	3.50±0.98	3.45±0.12	Y	3.526±0.329	3.338
113996	3.090±0.019	1	4.80±0.02	0.07	1.49±0.18	2.74±0.49	2.68±0.10	Y	2.759±0.253	3.246
114710	0.887±0.171	3	4.26±0.01	0.00	2.92±0.27	1.10±0.08	1.11±0.03	Y	1.104±0.118	1.125
117675	5.951±0.049	1	4.69±0.01	0.24	0.43±0.28	4.88±1.18	4.81±0.17	N	5.090±0.481	4.538
119228	4.338±0.117	3	4.66±0.02	0.13	0.34±0.18	5.17±0.78	5.11±0.15	Y	5.362±0.459	4.314
120136	0.822±0.049	1	4.50±0.01	0.02	3.51±0.35	0.80±0.23	0.81±0.03	N	0.831±0.963	0.891
120315	0.981±0.144	1	1.86±0.01	0.03	2.27±0.35	1.11±0.11	1.22±0.04	N	0.772±0.918	0.813
120477	4.691±0.022	1	4.05±0.02	0.01	0.44±0.18	4.65±0.75	4.56±0.16	Y	4.864±0.432	4.483
120933	5.932±0.042	1	4.75±0.02	0.22	-0.01±0.20	6.26±0.95	6.24±0.22	N	6.235±0.496	4.642
121130	6.799±0.077	1	4.66±0.02	0.09	-0.24±0.19	7.12±0.95	7.16±0.26	N	7.285±0.569	4.934
121370	2.134±0.012	5	2.68±0.01	0.02	1.49±0.17	2.09±0.36	2.11±0.06	Y	2.131±0.218	2.089
124850	1.222±0.061	3	4.08±0.01	0.07	2.80±0.27	1.14±0.10	1.16±0.03	Y	1.130±0.114	1.168
126660	0.902±0.097	3	4.05±0.01	0.02	2.74±0.33	1.19±0.17	1.20±0.04	Y	1.118±0.124	1.164
127665	3.901±0.008	1	3.58±0.01	0.05	0.76±0.17	3.65±0.61	3.57±0.13	Y	3.771±0.335	3.842
127762	1.726±0.011	3	3.04±0.01	0.04	2.51±0.38	1.16±0.17	1.22±0.04	Y	1.165±0.147	1.796
128167	0.714±0.205	3	4.47±0.00	0.03	3.34±0.32	0.88±0.12	0.89±0.03	Y	0.870±0.942	0.808

Table 9 continued on next page

Table 9 (*continued*)

Target	$\theta_{\text{LD,NPOI}}$		V	A_V	K	$\theta_{\text{LD,Mozur}}$	$\theta_{\text{LD,Adams}}$	Star	$\theta_{\text{LD,JMMC}}$	$\theta_{\text{LD,Gaia}}$
HD	(mas)	Ref	(mag)	(mag)	(mag)	(mas)	(mas)	in range?	(mas)	(mas)
129712	5.573±0.055	1	4.81±0.01	0.23	0.38±0.20	5.06±0.86	5.01±0.18	N	5.281±0.490	4.519
129989	4.840±0.010	2	2.38±0.01	0.06	0.12±0.20	4.53±0.83	4.46±0.16	Y	N/A	N/A
131873	10.229±0.012	2	2.08±0.01	0.08	-1.29±0.20	9.92±1.27	9.70±0.35	Y	10.154±0.796	9.777
132813	10.442±0.021	2	4.59±0.02	0.15	-0.96±0.20	10.38±1.18	10.68±0.38	N	N/A	5.549
133124	3.055±0.077	1	4.82±0.01	0.02	1.34±0.23	3.02±0.70	2.95±0.11	Y	2.936±0.283	3.200
133165	2.147±0.014	2	4.40±0.01	0.12	2.11±0.26	1.81±0.43	1.78±0.06	Y	1.751±0.167	2.088
133208	2.484±0.008	1	3.51±0.03	0.08	1.22±0.17	2.73±0.47	2.69±0.10	Y	2.767±0.290	3.034
135722	2.878±0.012	2	3.48±0.01	0.07	1.22±0.20	2.73±0.55	2.69±0.10	Y	2.981±0.242	3.233
136726	2.149±0.023	1	5.01±0.01	0.15	1.94±0.27	2.15±0.57	2.11±0.08	Y	2.142±0.194	2.246
137759	3.559±0.011	1	3.29±0.02	0.04	0.67±0.20	3.70±0.73	3.63±0.13	Y	3.840±0.288	3.694
140573	4.770±0.013	1	2.64±0.01	0.07	0.15±0.30	4.61±1.27	4.52±0.16	Y	4.686±0.467	3.996
141004	0.982±0.056	3	4.43±0.01	0.04	2.99±0.23	1.08±0.05	1.09±0.03	Y	1.062±0.831	1.063
141477	5.653±0.021	2	4.10±0.01	0.14	0.14±0.19	5.46±0.87	5.37±0.19	Y	5.666±0.492	4.719
142373	1.051±0.143	3	4.62±0.02	0.04	2.58±0.20	1.42±0.20	1.40±0.04	Y	1.359±0.945	0.964
143107	2.997±0.128	1	4.14±0.01	0.15	1.35±0.19	2.73±0.52	2.67±0.10	Y	2.752±0.249	3.076
146051	10.161±0.020	3	2.73±0.01	0.19	-1.17±0.21	9.87±1.31	9.69±0.29	N	10.245±0.748	9.621
146791	2.966±0.061	5	3.23±0.01	0.13	1.15±0.34	2.74±0.97	2.71±0.08	Y	2.918±0.332	2.819
148387	3.470±0.010	1	2.73±0.01	0.05	0.58±0.21	3.62±0.76	3.57±0.13	Y	3.750±0.293	3.635
148856	3.472±0.008	1	2.78±0.02	0.13	0.73±0.16	3.31±0.55	3.28±0.12	Y	3.422±0.243	2.002
150680	2.266±0.014	5	2.81±0.01	0.03	1.28±0.21	2.41±0.54	2.42±0.07	Y	N/A	2.416
150997	2.493±0.018	1	3.50±0.03	0.09	1.33±0.22	2.55±0.59	2.52±0.09	Y	2.636±0.268	3.056
153210	3.657±0.013	5	3.20±0.01	0.11	0.73±0.18	3.50±0.63	3.44±0.10	N	3.621±0.294	3.662
156283	5.159±0.011	1	3.16±0.02	0.22	-0.02±0.16	5.34±0.74	5.22±0.19	Y	5.711±0.353	5.771
159561	1.855±0.012	1	2.08±0.01	0.06	1.68±0.21	1.66±0.31	1.75±0.06	N	1.644±0.156	1.637
161096	4.511±0.011	1	2.77±0.01	0.11	0.44±0.18	3.93±0.69	3.87±0.14	Y	4.080±0.326	4.296
161797	1.880±0.008	1	3.42±0.01	0.03	1.51±0.20	2.29±0.47	2.27±0.08	N	2.345±0.174	2.238
161797	1.957±0.012	5	3.42±0.01	0.03	1.51±0.20	2.29±0.47	2.27±0.07	Y	2.345±0.174	2.238
163588	3.116±0.008	5	3.75±0.01	0.10	1.05±0.19	3.12±0.59	3.06±0.09	N	3.280±0.289	3.419
163917	2.789±0.005	1	3.34±0.00	0.21	1.23±0.31	2.62±0.83	2.59±0.09	Y	2.832±0.289	2.870
163993	2.206±0.017	2	3.70±0.01	0.16	1.49±0.21	2.36±0.50	2.33±0.08	Y	2.461±0.234	2.758
164058	10.190±0.015	2	2.23±0.01	0.16	-1.16±0.16	9.31±0.97	9.11±0.33	Y	9.421±0.682	9.112
168723	2.970±0.007	5	3.26±0.01	0.08	1.05±0.32	2.93±0.95	2.89±0.09	Y	3.141±0.331	3.640
169414	2.946±0.024	1	3.83±0.01	0.15	1.31±0.18	2.68±0.50	2.63±0.09	Y	2.763±0.286	3.234
170693	2.048±0.009	1	4.83±0.02	0.17	2.09±0.22	1.93±0.39	1.89±0.07	Y	1.913±0.152	2.036
172167	3.280±0.016	1	0.03±0.01	0.03	0.13±0.19	3.13±0.64	3.39±0.12	N	3.221±0.235	3.331
173667	0.905±0.022	3	4.20±0.01	0.08	3.19±0.26	0.92±0.07	0.94±0.03	Y	0.916±0.793	1.042
173764	2.223±0.011	3	4.22±0.01	0.87	1.62±0.29	2.12±0.63	2.12±0.06	N	2.191±0.215	2.361
175588	11.541±0.024	2	4.28±0.02	0.19	-1.26±0.18	11.86±1.10	12.18±0.44	N	12.280±0.884	0.882
176524	1.797±0.027	1	4.83±0.03	0.14	2.32±0.29	1.68±0.42	1.65±0.06	Y	1.589±0.152	1.821
176678	2.463±0.012	1	4.02±0.00	0.18	1.64±0.35	2.26±0.80	2.22±0.08	Y	2.349±0.272	2.686
180610	1.630±0.028	1	4.98±0.01	0.18	2.15±0.25	1.89±0.44	1.86±0.07	Y	1.885±0.198	1.796
180809	2.357±0.045	3	4.37±0.01	0.16	1.51±0.22	2.54±0.56	2.49±0.07	N	2.553±0.228	2.502
181276	2.143±0.008	1	3.79±0.02	0.13	1.76±0.19	2.05±0.38	2.03±0.07	Y	2.133±0.198	2.316
181907	1.089±0.023	5	5.82±0.01	0.42	3.46±0.26	0.94±0.05	0.93±0.03	N	1.026±0.911	1.071
182640	1.203±0.016	4	3.36±0.01	0.07	2.44±0.25	1.27±0.18	1.31±0.05	N	1.290±0.119	1.196
183439	4.403±0.020	1	4.44±0.02	0.27	0.71±0.21	4.03±0.80	3.95±0.14	Y	4.223±0.430	4.553

Table 9 continued on next page

Table 9 (*continued*)

Target	$\theta_{\text{LD,NPOI}}$		V	A_V	K	$\theta_{\text{LD,Mozur}}$	$\theta_{\text{LD,Adams}}$	Star	$\theta_{\text{LD,JMMC}}$	$\theta_{\text{LD,Gaia}}$
HD	(mas)	Ref	(mag)	(mag)	(mag)	(mas)	(mas)	in range?	(mas)	(mas)
183912	4.904±0.035	3	3.09±0.01	0.14	0.39±0.21	4.19±0.85	4.10±0.12	N	N/A	5.709
184406	2.032±0.040	3	4.45±0.01	0.15	1.70±0.27	2.30±0.63	2.26±0.07	N	2.433±0.261	2.401
186791	7.056±0.080	1	2.72±0.01	0.30	-0.72±0.24	7.51±1.34	7.35±0.26	Y	7.370±0.677	1.974
187642	3.309±0.006	1	0.77±0.02	0.02	0.10±0.25	3.62±0.94	3.75±0.14	N	3.577±0.338	3.403
187929	1.804±0.007	1	3.73±0.14	0.00	1.79±0.22	2.02±0.53	2.00±0.07	N	1.879±0.139	N/A
187929	1.808±0.055	4	3.73±0.14	0.00	1.79±0.22	2.02±0.53	2.00±0.07	N	1.879±0.139	N/A
188310	1.658±0.025	1	4.70±0.02	0.25	2.17±0.22	1.78±0.36	1.75±0.06	Y	1.785±0.134	1.775
188512	2.166±0.009	5	3.72±0.01	0.06	1.71±0.23	2.10±0.48	2.08±0.06	Y	2.112±0.177	2.393
189319	6.089±0.011	2	3.48±0.03	0.27	-0.23±0.01	6.20±0.15	6.07±0.22	Y	N/A	5.886
192909	5.557±0.015	2	3.98±0.01	0.28	0.18±0.01	5.18±0.05	5.08±0.18	Y	N/A	4.640
196094	4.472±0.017	1	4.61±0.02	0.68	0.71±0.21	3.92±0.77	3.83±0.14	Y	N/A	N/A
197989	4.985±0.046	2	2.46±0.01	0.08	-0.01±0.20	4.93±0.91	4.84±0.17	Y	4.976±0.369	4.499
198001	0.503±0.357	4	3.77±0.01	0.19	3.74±0.22	0.59±0.36	0.64±0.02	N	0.561±0.517	0.587
198026	7.079±0.088	2	4.43±0.01	0.32	-0.26±0.36	6.90±1.83	6.86±0.25	N	7.127±0.857	5.086
198149	2.518±0.009	3	3.42±0.01	0.04	1.39±0.24	2.45±0.60	2.43±0.07	Y	2.540±0.235	3.150
200905	5.816±0.010	2	3.73±0.04	0.25	-0.04±0.20	5.73±0.97	5.61±0.20	Y	5.764±0.454	4.551
202444	2.169±0.028	3	3.73±0.01	0.06	2.55±0.28	1.27±0.19	1.29±0.04	Y	N/A	N/A
203280	1.677±0.007	3	2.45±0.01	0.04	2.07±0.24	1.40±0.24	1.47±0.04	Y	1.432±0.144	1.424
203504	2.315±0.023	1	4.09±0.01	0.18	1.75±0.21	2.13±0.45	2.10±0.08	Y	2.172±0.197	2.509
204867	2.704±0.009	1	2.90±0.02	0.26	1.21±0.28	2.46±0.72	2.47±0.09	N	2.530±0.241	2.949
205435	1.977±0.036	3	4.01±0.01	0.12	1.90±0.32	1.94±0.60	1.92±0.06	Y	1.956±0.275	2.040
206952	1.819±0.015	1	4.56±0.01	0.17	1.72±0.20	2.30±0.47	2.26±0.08	Y	2.243±0.159	1.991
208816	7.251±0.012	2	4.94±0.06	1.77	0.00±0.18	5.41±0.87	5.29±0.19	N	6.333±0.615	5.584
209750	3.066±0.036	1	2.94±0.02	0.26	0.59±0.21	3.60±0.78	3.55±0.13	Y	3.394±0.319	6.200
210418	0.688±0.031	4	3.52±0.02	0.10	3.38±0.26	0.72±0.26	0.77±0.03	N	0.690±0.632	1.079
210745	5.302±0.023	2	3.35±0.01	0.32	0.34±0.17	4.36±0.69	4.27±0.15	Y	4.415±0.358	6.651
211388	3.371±0.049	1	4.14±0.02	0.18	1.01±0.22	3.31±0.71	3.24±0.12	Y	3.369±0.286	3.749
212496	1.957±0.037	1	4.44±0.01	0.18	1.88±0.22	2.06±0.44	2.03±0.07	Y	2.056±0.162	2.065
213306	1.526±0.018	2	3.56±0.10	0.36	2.35±0.22	1.33±0.22	1.36±0.05	N	1.359±0.174	0.089
213311	5.881±0.022	1	4.37±0.01	0.53	0.27±0.21	5.01±0.93	4.91±0.18	N	5.313±0.445	4.704
214868	2.555±0.047	2	4.48±0.02	0.15	1.67±0.22	2.36±0.52	2.31±0.08	Y	2.391±0.241	2.800
215182	3.471±0.027	1	2.95±0.01	0.15	1.02±0.23	2.83±0.68	2.81±0.10	N	2.921±0.246	2.610
216131	2.508±0.125	2	3.49±0.01	0.09	1.18±0.16	2.79±0.45	2.75±0.10	Y	2.856±0.252	2.985
216386	8.333±0.042	2	3.75±0.03	0.14	-0.67±0.33	8.27±1.81	8.20±0.30	N	8.377±0.913	4.369
218329	4.234±0.009	1	4.53±0.02	0.15	0.61±0.32	4.37±1.27	4.29±0.15	Y	4.573±0.491	4.441
218452	1.991±0.047	2	5.32±0.01	0.12	2.11±0.28	2.03±0.53	1.98±0.07	Y	2.024±0.187	2.080
219215	5.221±0.029	1	4.22±0.01	0.14	-0.10±0.35	6.31±1.69	6.24±0.22	N	6.240±0.726	4.882
219449	2.220±0.031	1	4.23±0.01	0.12	1.60±0.24	2.39±0.57	2.35±0.08	Y	2.432±0.222	2.235
219615	2.482±0.012	1	3.70±0.01	0.11	1.39±0.25	2.52±0.66	2.48±0.09	Y	N/A	2.783
221115	1.432±0.104	3	4.55±0.02	0.11	2.44±0.35	1.51±0.41	1.50±0.04	Y	1.481±0.173	1.635
222107	2.772±0.012	3	3.82±0.03	0.09	1.47±0.22	2.46±0.57	2.42±0.07	N	2.473±0.198	3.057
222404	3.254±0.020	1	3.21±0.01	0.05	1.04±0.21	2.94±0.63	2.90±0.10	Y	3.000±0.347	3.053
224014	2.562±0.043	3	4.51±0.08	0.00	1.67±0.21	2.41±0.55	2.36±0.07	N	2.162±0.191	N/A
224935	8.007±0.059	2	4.40±0.00	0.13	-0.40±0.22	7.58±1.14	7.59±0.27	N	7.914±0.588	5.395

Table 9 continued on next page

Table 9 (*continued*)

Target	$\theta_{\text{LD,NPOI}}$	V	A_V	K	$\theta_{\text{LD,Mozur}}$	$\theta_{\text{LD,Adams}}$	Star	$\theta_{\text{LD,JMMC}}$	$\theta_{\text{LD,Gaia}}$
HD	(mas)	Ref	(mag)	(mag)	(mas)	(mas)	in range?	(mas)	(mas)

NOTE—Two stars appear in the table twice, having been published in two different NPOI papers: HD 161797 and HD 187929.

$\theta_{\text{LD,NPOI}}$ is the NPOI limb-darkened angular diameter from the following sources: 1. [Baines et al. \(2018\)](#); 2. [Baines et al. \(2021\)](#); 3. here; 4. [Baines et al. \(2023\)](#); and 5. [Baines et al. \(2014\)](#).

V magnitudes are from [Mermilliod \(1991\)](#).

K magnitudes are from [Cutri et al. \(2003\)](#) for all stars except HD 189319 and HD 192909, which are from [Richichi et al. \(2005\)](#) and have an assigned error of 0.01.

A_V is from [Gontcharov & Mosenkov \(2018\)](#), for all but 9 stars. For those, we used: [Salsi et al. \(2020\)](#), HD 10700, HD 19373, HD 61421, and HD 114710), [Neckel et al. \(1980\)](#), HD 31964), [Le Borgne et al. \(2003\)](#), HD 187929), [Famaey et al. \(2005\)](#), HD 196094, HD 208816, and HD 213311). HD 224014 had no A_V listed on Vizier.

$\theta_{\text{LD,Mozur}}$ is the angular diameter calculated using equations from [Mozurkewich et al. \(2003\)](#), $\theta_{\text{LD,Adams}}$ is from [Adams et al. \(2018\)](#), $\theta_{\text{LD,JMMC}}$ is from the *JMMC Stellar Diameters Catalog* ([Bourg  s et al. 2014](#)), and $\theta_{\text{LD,Gaia}}$ is from [Gaia Collaboration et al. \(2018\)](#).

The Y/N in the “Star in range?” column indicates whether or not the particular star was within the color limits of [Adams et al. \(2018\)](#) and is included in Figure 6. See Section 6 for details.

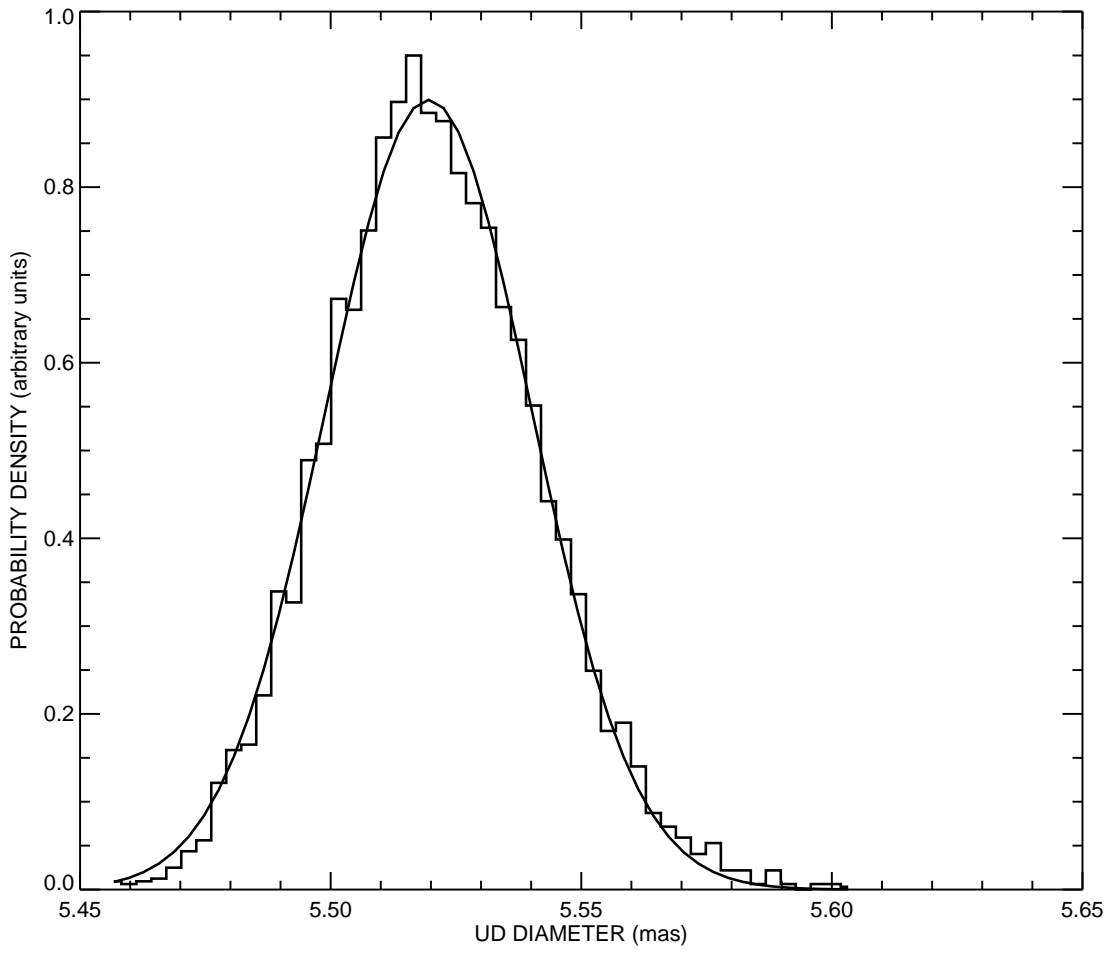


Figure 1. An example probability density solution for the diameter fit to HD 3712/α Cas visibilities as described in Section 3.

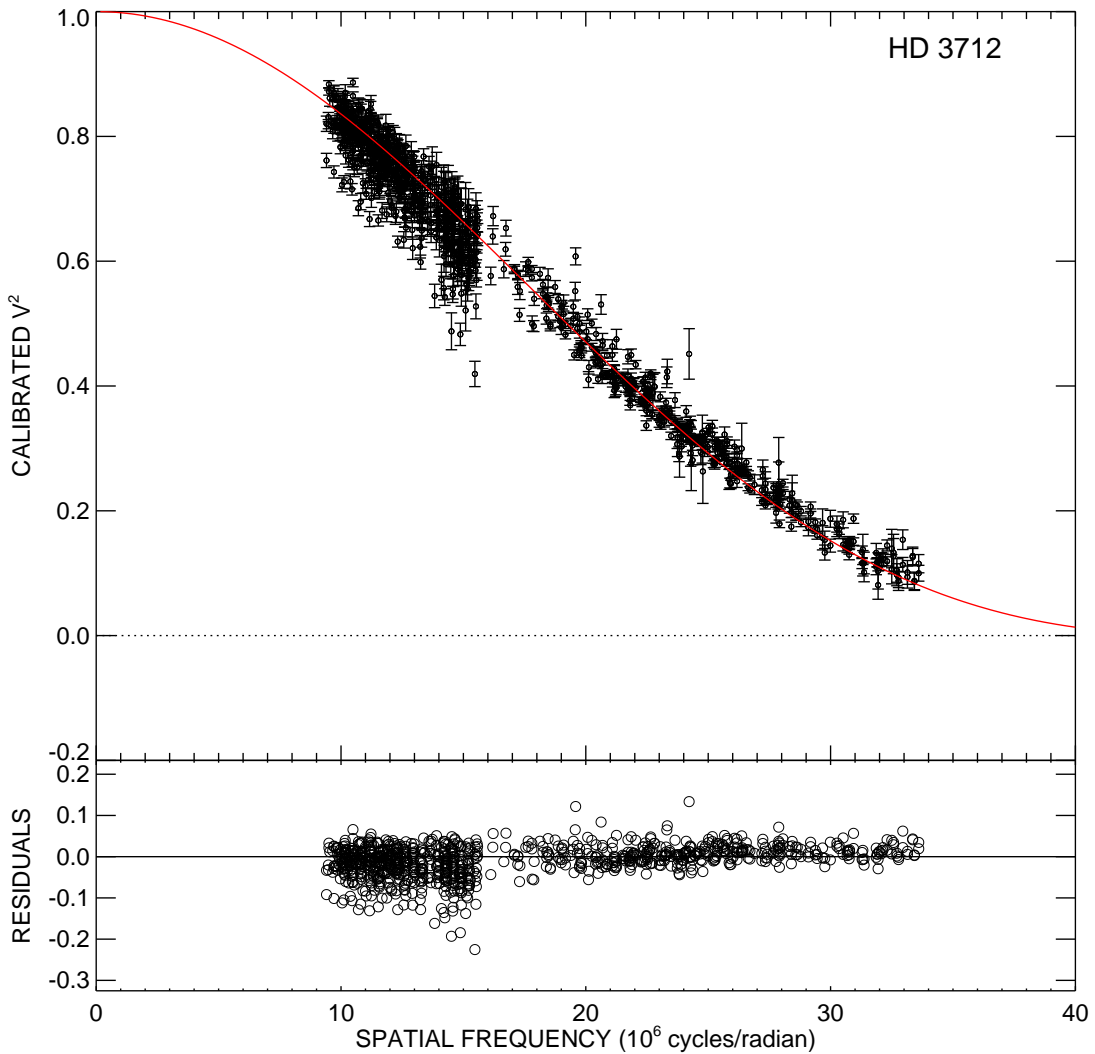


Figure 2. *Top panel:* The θ_{LD} fit for HD 3712/ α Cas. The solid red line represents the visibility curve for the best fit θ_{LD} , the points are the calibrated visibilities, and the vertical lines are the measurement uncertainties. *Bottom panel:* The residuals (O-C) of the diameter fit to the visibilities. The plots for the remaining stars are available on the electronic version of the *Astronomical Journal*.

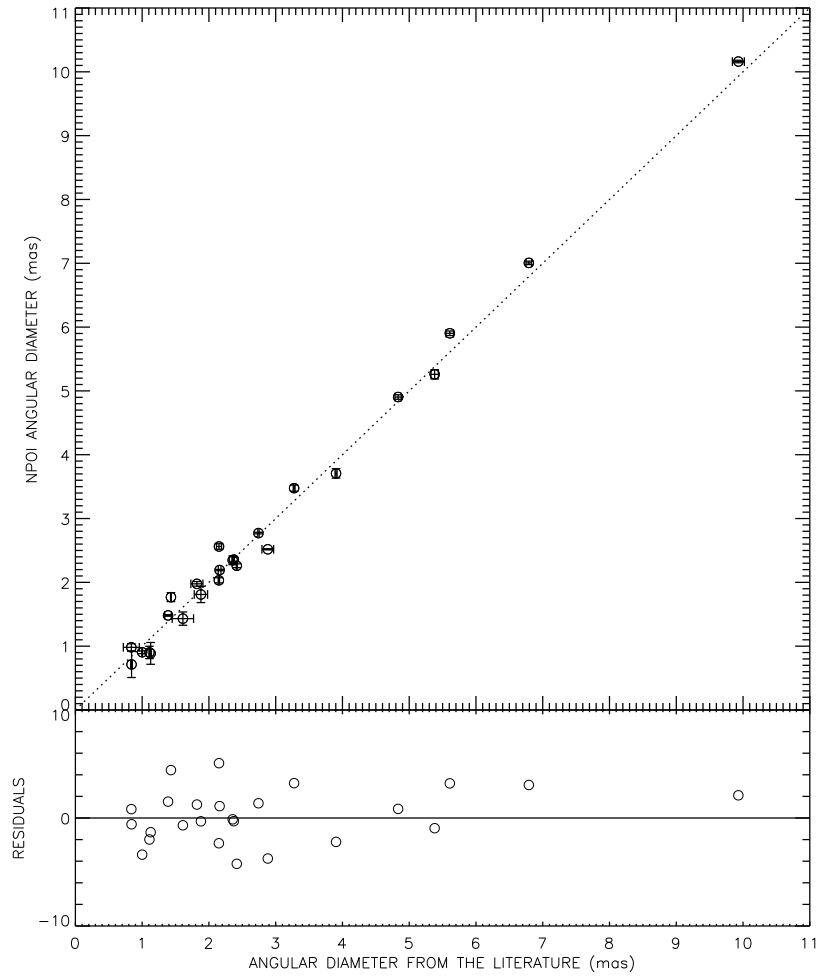


Figure 3. *Top panel:* Comparison of the angular diameters measured here versus previously measured interferometric diameters from the literature. The error bars are included but are often smaller than the open circle indicating the measurement. The dotted line is the 1:1 ratio. When more than one measurement was available in the literature, we used the most recent measurement (see Table 8). *Bottom panel:* The residuals were calculated as follows: $(\theta_{\text{NPOI}} - \theta_{\text{literature}}) \times (\text{combined error})^{-1}$.

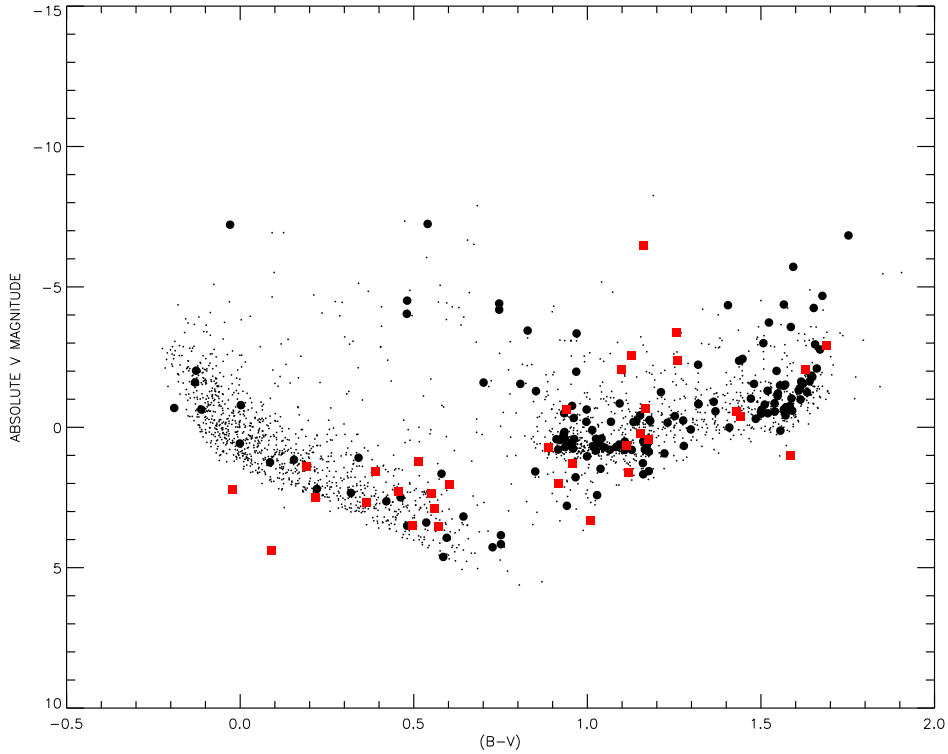


Figure 4. A color-magnitude diagram of our new stars (red squares), past NPOI targets (large black circles), and targets from *JMMC* (Bourg  s et al. 2014, small black points) that fall within the limits of the NPOI observable range of declination higher than -10 deg and brighter than $V = 6.0$.

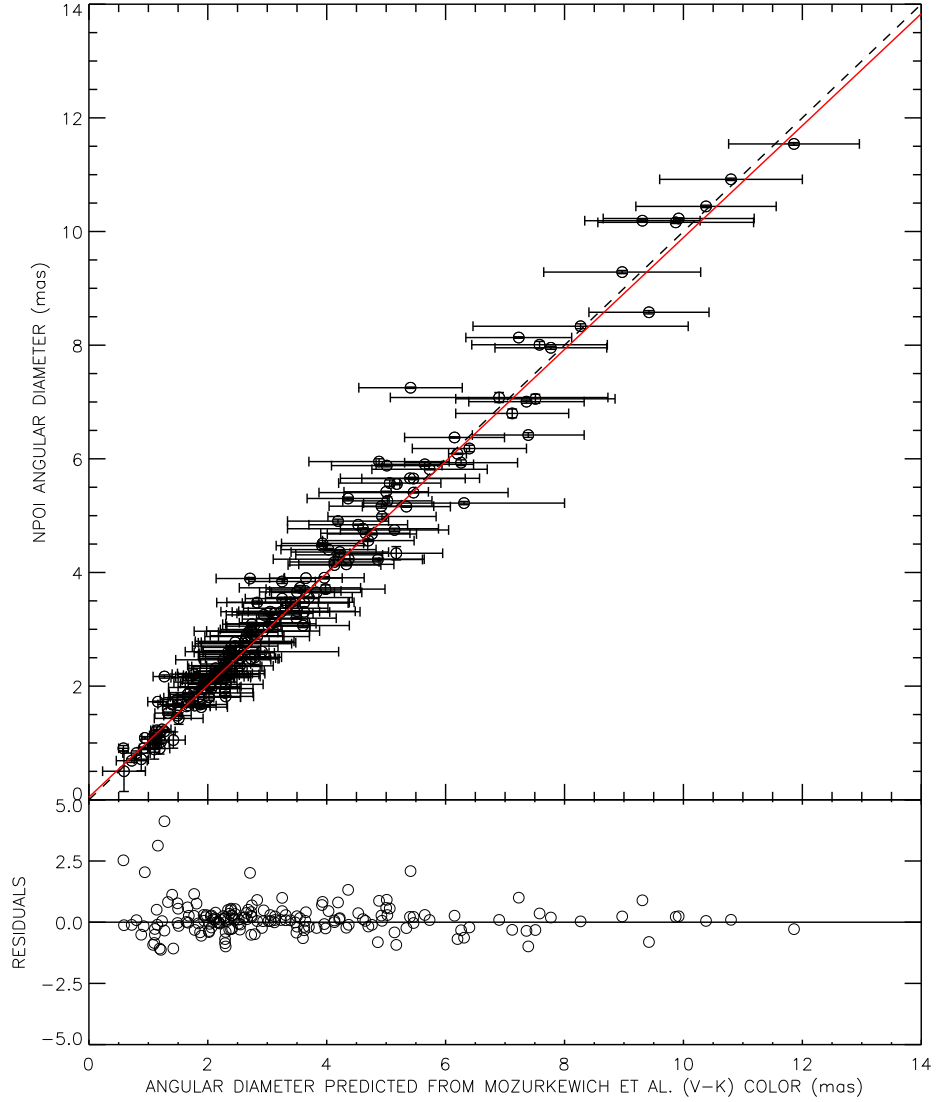


Figure 5. *Top panel:* Comparison of the angular diameters measured here versus diameters predicted using the relations from the [Mozurkewich et al. \(2003\)](#) paper (Eq. 3 and 4 in Section 6). Note that the NPOI errors are often smaller than the open circle indicating the data point, and are almost universally much smaller than that predicted using $(V - K)$ color. The black dashed line is the 1:1 ratio, and the solid red line is the linear fit to the data ($f(x) = 1.001x + 0.068$). *Bottom panel:* The residuals to the 1:1 fit, calculated as described in Figure 3.

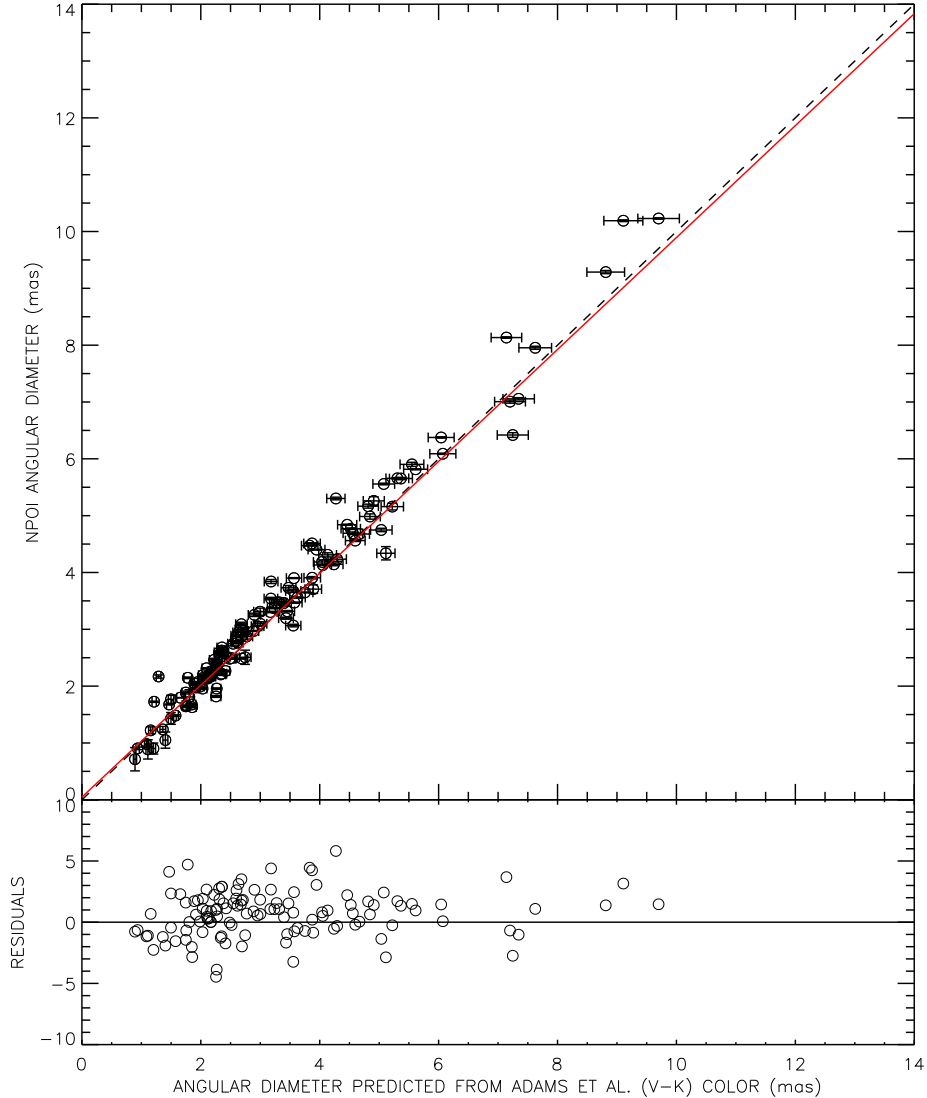


Figure 6. *Top panel:* Comparison of the angular diameters measured here versus diameters predicted using the relations from the Adams et al. (2018) paper. As in Figure 5, NPOI errors are often smaller than the open circle indicating the data point, as is the case for some of the diameters predicted using $(V - K)$ color. The dotted line is the 1:1 ratio, and the solid red line is the linear fit to the data ($f(x) = 1.039x - 0.014$). *Bottom panel:* The residuals to the 1:1 line, calculated in the same way as described in Figure 3.

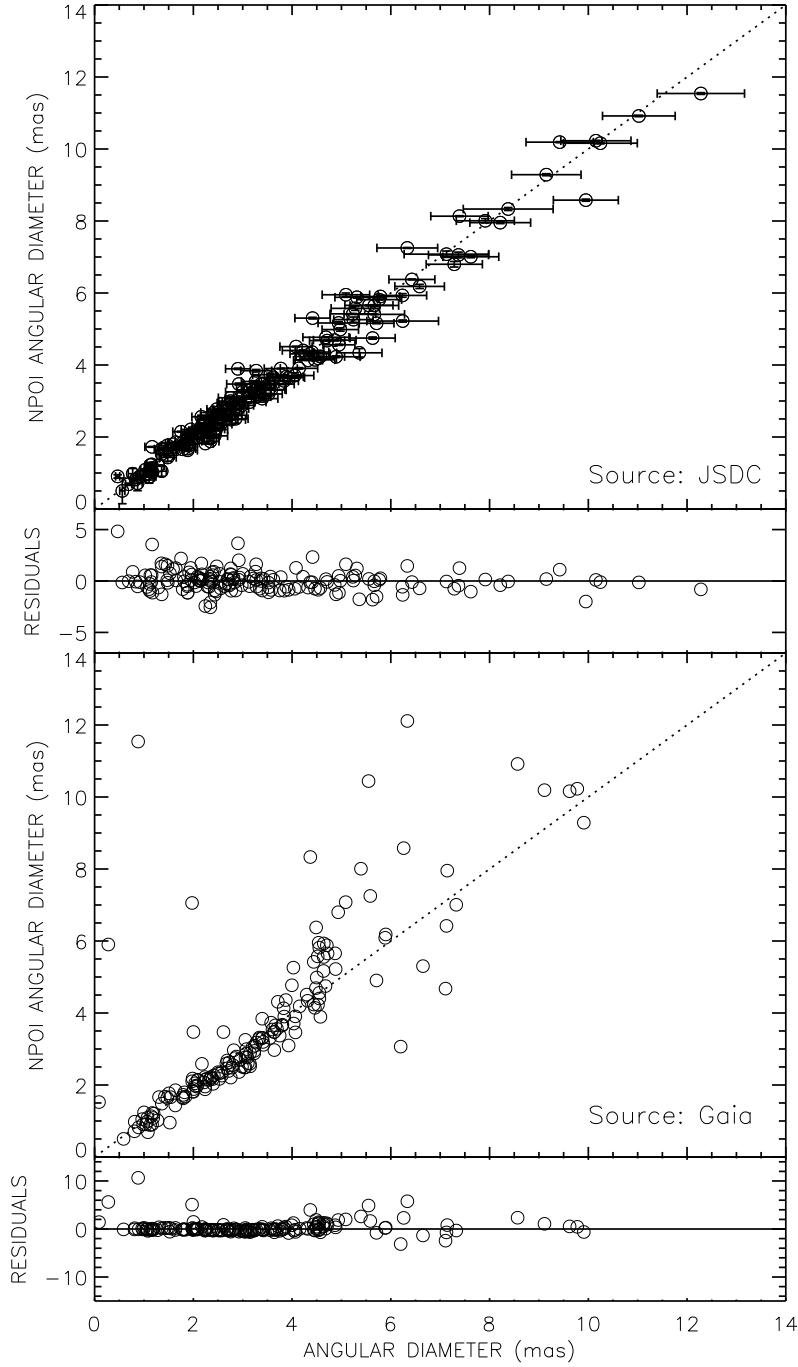


Figure 7. *Top panel:* Comparison of the limb-darkened angular diameters measured here versus diameters from *JMMC* (Bourg  s et al. 2014). The linear fit is $f(x) = 0.969x + 0.088$. *Bottom panel:* The same, but from *Gaia* (Gaia Collaboration et al. 2018; Cruzal  bes et al. 2019), with a linear fit of $f(x) = 0.996x + 0.246$. Note that no errors were indicated for the *Gaia* diameters, so the residuals are simply $\theta_{\text{NPOI}} - \theta_{\text{GAIA}}$.